FAM84B promotes prostate tumorigenesis through a network alteration

Yanzhi Jiang, Xiaozeng Lin, Anil Kapoor, Lizhi He, Fengxiang Wei, Yan Gu, Wenjuan Mei, Kuncheng Zhao, Huixiang Yang* and Damu Tang

Ther Adv Med Oncol

2019, Vol. 11: 1–27

DOI: 10.1177/1758835919846372

Abstract

Background: The aim of this study was to investigate the contributions of FAM84B in prostate tumorigenesis and progression.

Methods: A FAM84B mutant with deletion of its HRASLS domain (ΔHRASLS) was constructed. DU145 prostate cancer (PC) cells stably expressing an empty vector (EV), FAM84B, or FAM84B (ΔHRASLS) were produced. These lines were examined for proliferation, invasion, and growth in soft agar *in vitro.* DU145 EV and FAM84B cells were investigated for tumor growth and lung metastasis in NOD/SCID mice. The transcriptome of DU145 EV xenografts ($n = 2$) and DU145 FAM84B tumors ($n = 2$) was determined using RNA sequencing, and analyzed for pathway alterations. The FAM84B-affected network was evaluated for an association with PC recurrence.

Results: FAM84B but not FAM84B (ΔHRASLS) increased DU145 cell invasion and growth in soft agar. Co-immunoprecipitation and co-localization analyses revealed an interaction between FAM84B and FAM84B (ΔHRASLS), suggesting an intramolecular association among FAM84B molecules. FAM84B significantly enhanced DU145 cell-derived xenografts and lung metastasis. In comparison with DU145 EV cell-produced tumors, those generated by DU145 FAM84B cells showed a large number of differentially expressed genes (DEGs; $n = 4976$). A total of 51 pathways were enriched in these DEGs, which function in the Golgi-to-endoplasmic reticulum processes, cell cycle checkpoints, mitochondrial events, and protein translation. A novel 27-gene signature (SigFAM) was derived from these DEGs; SigFAM robustly stratifies PC recurrence in two large PC populations ($n = 490$, $p = 0$; $n = 140$, $p = 4e^{-11}$), and remains an independent risk factor of PC recurrence after adjusting for age at diagnosis, Gleason scores, surgical margin, and tumor stages.

Conclusions: FAM84B promotes prostate tumorigenesis through a complex network that predicts PC recurrence.

Keywords: biomarkers, FAM84B, prostate cancer, prostate cancer recurrence

Received: 30 November 2018; revised manuscript accepted: 13 March 2019.

Correspondence to:
Damu Tang
Department of Medicine, McMaster University, T3310, St. Joseph's Hospital, 50 Charlton Avenue East, Hamilton, ON, L8N 4A6, Canada
damut@mcmaster.ca

Yanzhi Jiang
Department of Gastroenterology, Xiangya Hospital, Central South University, Changsha, Hunan, China
Department of Medicine, McMaster University, Hamilton, ON, Canada
Father Sean O'Sullivan Research Institute, St. Joseph's Hospital, Hamilton, ON. Canada
Hamilton Center for Kidney Research, St. Joseph's Hospital, Hamilton, ON, Canada
Hamilton Urologic Urological Cancer Center for Research and Innovation (UCCRI), St. Joseph's Hospital, Hamilton, ON, Canada

Xiaozeng Lin
Yan Gu
Kuncheng Zhao
Department of Medicine, McMaster University, Hamilton, ON, Canada
Father Sean O'Sullivan Research Institute, St. Joseph's Hospital/ Hamilton Center for Kidney Research, St. Joseph's Hospital, Hamilton, ON, Canada
Urological Cancer Center for Research and Innovation (UCCRI), St. Joseph's Hospital, Hamilton, ON, Canada

Anil Kapoor
Father Sean O'Sullivan Research Institute, St. Joseph's Hospital, Hamilton, ON, Canada
Urological Cancer Center for Research and Innovation (UCCRI), St. Joseph's Hospital, Hamilton, ON, Canada
Department of Surgery,

Introduction

Prostate cancer (PC) is the most frequently diagnosed male malignancy in the developed world.[1] PC evolves from high grade prostatic intra-epithelial neoplasia lesions which may progress to metastasis diseases.[2] Primary PCs are managed by a variety of treatment options including active surveillance, surgery, and radiation; treatment choices consider multiple factors such as disease severity, patient age and preference. The severity of PCs is graded using the Gleason score (GS) and GS-based World Health Organization (WHO) PC grading system (WHO grade group 1–5) or its equivalent ISUP (the International Society of Urological Pathology) grade.[3–5] Aproximately 30% of tumors will relapse following surgery, evident by an increase in serum prostate-specific antigen (PSA), a process that is known as biochemical recurrence (BCR).[6] The recurrence is a major progression of PC, which often results in poor prognosis; a large percentage of relapsed PCs will progress to metastatic

McMaster University, Hamilton, Ontario, Canada

Lizhi He
Harvard Medical School and Massachusetts General Hospital, Boston, MA, USA

Fengxiang Wei
The Genetics Laboratory, Longgang District Maternity and Child Healthcare Hospital, Longgang District, Shenzhen, Guangdong, China

Wenjuan Mei
Department of Medicine, McMaster University, Hamilton, ON, Canada
Father Sean O'Sullivan Research Institute, St. Joseph's Hospital
Hamilton Center for Kidney Research, St. Joseph's Hospital, Hamilton, ON, Canada
Urological Cancer Center for Research and Innovation (UCCRI), St. Joseph's Hospital, Hamilton, ON, Canada
Department of Nephrology, The First Affiliated Hospital of Nanchang University, Jiangxi, China

Huixiang Yang
Department of Gastroenterology, Xiangya Hospital, Central South University, Changsha, Hunan, China

*Huixiang Yang is the co-corresponding author

disease.[7] With a few exceptions, metastases remain incurable. Metastatic PCs are managed with androgen-deprivation therapy, which was based on the seminal discovery of PC proliferation relying on androgen signaling in the 1940s.[8,9] Nonetheless, metastatic castration-resistant PC (mCRPC) inevitably occurs.[10,11] Although mCRPC can be treated with taxane-based chemotherapy, androgen receptor (AR)-targeting therapy involving either abiraterone or enzalutamide,[11–13] and immunotherapy,[14,15] these treatments offer modest benefits in these patients.[11,16] The progression of PC is regulated by complex networks, of which our understanding remains limited.

PC tumorigenesis and progression are promoted by the growth factor phosphoinositide 3-kinase (PI3K) pathway, androgen receptor signaling, cell cycle regulators, Myc, and others.[17,18] Myc is amplified in PC,[19] which initiates the PC process in mice[17] and is associated with PC recurrence and poor prognosis in patients.[20–22] Myc is well known to collaborate with Ras during tumorigenesis[23–25]; this collaboration induces hyperplasia in the prostate.[26]

The newly identified PC factor, FAM84B, displays potential connections with both Myc and Ras. The *FAM84B* and *Myc* genes are at the chromosomal locus 8q24.21 bordering the centromeric and telomeric end of a 1.2 Mb gene desert region respectively.[27–31] Amplification of 8q24 occurs most frequently in human cancers, including ovarian,[32] colorectal,[30,33–35] breast,[28,36–39] prostate,[27,29,31,40–42] and others. This structural setting suggests a connection between Myc and FAM84B; however, while the oncogenic involvement of Myc has been extensively investigated, the same can hardly be claimed for FAM84B. FAM84B elevation was recently shown to be associated with poor prognosis in esophageal squamous cell carcinoma,[43,44] and with PC progression.[45]

Ras is a potent oncogene regulated by an array of factors. The H-Ras-like suppressor (HRASLS) family consists of five members (HRASLS1-5) in humans, which all possess tumor suppression activities and can repress H-Ras-initiated oncogenic events *in vitro*.[46] The family has a typical LRAT (lecithin:retinal acyltransferase) homologous domain.[46] We observed that FAM84B contains a LRAT domain and a subregion within this domain that shares a high level of homology to HRASLS1-5. While overexpression of FAM84B elevated DU145 cell invasion and growth in soft agar *in vitro*, removal of this subregion abolished these activities. Additionally, FAM84B overexpression promoted the growth of xenografts produced by DU145 cells. The enhancement is associated with alterations of a network consisting of 4976 differentially expressed genes (DEGs), which contribute to the enrichment of 51 pathways regulating the Golgi–endoplasmic reticulum (ER) process, cell cycle checkpoints, protein translation and mitochondrial events. Furthermore, these DEGs contain a multigene signature that robustly predicts PC recurrence in two large independent cohorts. Collectively, we provide evidence for FAM84B stimulating PC tumorigenesis likely through a network change.

Methods

Cell culture, plasmids, and stable line construction

DU145 cells were purchased from American Type Culture Collection (ATCC), and cultured in Minimum Essential Media (MEM) supplemented with 5% fetal bovine serum (FBS) (Sigma Aldrich, Oakville, ON, Canada) and 1% penicillin-streptomycin (Thermo Fisher Scientific, Burlington, ON, Canada). The cell line was authenticated (Cell Line Authentication Service, ATCC), and routinely tested for *Mycoplasma* contamination using a polymerase chain reaction (PCR) kit (Abm, Cat#: G238, Toronto, ON, Canada). The FAM84B mutant with deletion of the HRASLS domain was constructed using PCR. Briefly, the fragments N-terminal and C-terminal to the deletions region were amplified using PCR and then ligated together into a retroviral vector. DU145 empty vector (EV/pBabe), FAM84B, or the FAM84B mutant stable lines were constructed using retrovirus as previously described.[47] Briefly, a gag-pol, an envelope (VSV-G; Stratagene), and a designed retroviral vector (EV, FAM84B, or its mutant) were transiently co-transfected into 293T cells at the ratio 1:1:1. At 48 hours post transfection, the virus-containing medium was filtered (0.45-μM filter) and centrifuged (50,000*g*) for 90 min. The retrovirus pellets were resuspended into medium supplemented with 10 μg/ml of polybrene (Sigma Aldrich, Oakville, ON, Canada). DU145 cells were subsequently infected and selected with puromycin; Stable lines (without selection for single-cell clones) were used as pool populations in this research.

Invasion assay

Transwell was used for invasion assay. Insert chambers with either a control membrane or a Matrigel membrane (8-μM pore size) for 24-well plates were purchased (Life Sciences Corning® BioCoat™, USA). Assay was carried out according to the manufacturer's instructions. Cells (10^4) were seeded into the top chamber with serum-free medium; medium containing 5% FBS was added to the bottom chambers. Cells going through the membrane were stained with crystal violet (0.5%) and counted.

Soft agar assay

Six-well tissue culture plates were first coated with a bottom layer agar, 2 ml of 0.6% agar dissolved in complete tissue culture medium. Cells (10^4) in 2 ml of 0.35% agar dissolved in complete cell culture medium were then seeded on the solidified bottom layer. Cells were cultured for approximately 3 weeks in a tissue culture incubator with moisture by adding 100 μl of complete medium weekly.

Colony formation assay and proliferation assay

Growth curves were constructed by seeding cells into six-well tissue culture plates (10^5 per well), followed by counting cells daily. Colony formation assays were performed by seeding cells in six-well plates at the designed density; colonies were stained with crystal violet (0.5%) after culture for 2 weeks. Colony numbers were counted and analyzed.

Immunofluorescence staining

Immunofluorescence (IF) staining was performed by fixing cells with paraformaldehyde for 20 min, followed by permeabilization with 0.3% Triton X-100 for 15 min. Cells were then blocked with a blocking buffer (3% donkey serum + 3% bovine serum albumin (BSA) + 0.3% Triton X-100 in PBS) prior to the addition of primary antibodies polyclonal anti-FLAG (a commonly used polypeptide epitope tag) (1:100, Sigma) and monoclonal anti-HA (a tag epitope derived from hemagglutinin) (12CA5, 1:10 of hybridoma conditional medium) at 4°C overnight. After rinsing with PBS, secondary antibodies FITC (fluorescein)-donkey anti-mouse immunoglobulin (Ig)G (1:200, Jackson Immuno Research Lab) and rhodamine-donkey anti-rabbit IgG (1:200, Jackson Immuno Research Lab) were applied for 1 h at room temperature. Slides were eventually mounted using VECTASHIELD mounting medium containing 4′,6-diamidino-2-phenylindole (DAPI; VECTOR Lab Inc.). Images were taken with a fluorescent microscope (Axiovert 200, Carl Zeiss).

Immunoprecipitation (IP)

IP was carried out by incubating cell lysates containing 1 mg of protein with individual antibodies and Protein G agarose (Invitrogen) overnight at 4°C, followed by eight washes with a buffer [50 mM Tris (pH 7.5), 100 mM NaCl, 7.5 mM ethylene glycol-bis(β-aminoethyl ether)-*N,N,N′,N′*-tetraacetic acid [EGTA], and 0.1% Triton X-100]. Antibodies used for IP were monoclonal anti-HA (12CA5, 1:10 of hybridoma conditional medium) and anti-M2 (1 μg, Sigma). Antibodies used for the western blot were polyclonal anti-FLAG (1:500, Sigma) and polyclonal anti-HA (1:500, Santa Cruz).

Formation of xenograft tumors and lung metastases

Xenografts were generated as previously described.[47–50] Briefly, DU145 EV or DU145 FAM84B cells (3×10^6) in 0.1 ml culture media were mixed with Matrigel mixture (BD) at 1:1 (volume : volume), and implanted (one graft/mouse) subcutaneously (s.c.) into the flank of NOD/SCID mice (6-week-old males, $n = 5$ per group; The Jackson Laboratory). Tumor growth was monitored through observation and palpation; tumor size was measured every 5 days using calipers. Tumor volume was calculated as $V = L \times W^2 \times 0.52$. Animals were sacrificed when tumors reached a volume $\geqslant 1000\,mm^3$. Lung metastases were produced *via* tail vein injection of DU145 EV or DU145 FAM84B cells (10^6) into NOD/SCID mice. Endpoints were defined by a weight loss ⩾10%. All animal experiments were performed according to the protocols approved by the McMaster University Animal Research Ethics Board (AUP#: 16-06-24).

Western blot analysis

Cell lysates were prepared in a lysate buffer [20 mM Tris (pH 7.4), 150 mM NaCl, 1 mM ethylenediaminetetraacetic acid (EDTA), 1 mM EGTA, 1% Triton X-100, 25 mM sodium pyrophosphate, 1 mM NaF, 1 mM β-glycerophosphate, 0.1 mM sodium orthovanadate, 1 mM phenylmethylsulfonyl fluoride

(PMSF), 2 μg/ml leupeptin and 10 μg/ml aprotinin]. A total 50 μg of cell lysate protein was separated on sodium dodecyl sulfate-polyacrylamide gel electrophoresis (SDS-PAGE) gel and transferred onto Hybond ECL nitrocellulose membranes (Amersham), followed by blocking with 5% skimmed milk at room temperature for 1 h. Primary antibodies were added overnight at 4°C with agitation, followed by incubation with secondary antibodies for 1 hour at room temperature. Signals were subsequently developed (ECL Western Blotting Kit, Amersham). Primary antibodies used were: anti-FAM84B 1:2000 (Proteintech), anti-phospho-AKT (serine 473; Signaling Technology, 9271S, 1:500), anti-AKT (Santa Cruz Biotechnology, sc-1618, 1:1000), anti-BAD (Abcam, ab32445, 1:2000), anti-FLAG (Sigma Aldrich, F3165, 1:1000), anti-actin (Santa Cruz Biotechnology, sc-1615, 1:1000), and anti-tubulin 1:1000 (Santa Cruz).

Quantification of FAM84B mRNA expression using real-time PCR

Total RNA was isolated from either cells or xenograft tissues with the Isol-RNA Lysis Reagent (5 PRIME); reverse transcription was performed using Superscript III (Thermo Fisher Scientific). Quantitative real-time PCR was performed using the ABI 7500 Fast Real-Time PCR System (Applied Biosystems) using SYBR-green (Thermo Fisher Scientific) with the following primers: FAM84B forward 5'-GACCCAC CTAAGTTACAAGGAAG-3', and reverse 5'- GTA GAACACGGAGCATTCCAC-3'; β-Actin forward 5'-TGAAGGTGACAGCAGTCGGT-3', and reverse 5'-TAGAGAGAAGTGGGGTGGCT-3'. Data analysis was performed using the formula: $2^{-\Delta\Delta Ct}$.

Immunohistochemistry (IHC)

Slides were deparaffinized in xylene and cleared in an ethanol series. Antigens were retrieved in sodium citrate buffer (pH = 6.0) by the method of heat activation. Slides were blocked in PBS containing 1% BSA and 10% normal goat serum (Vector Laboratories) for 1 hour and incubated with anti-FAM84B antibody (1:350, Proteintech) overnight at 4°C. Secondary antibody (biotinylated goat anti-rabbit IgG) and Vector ABC reagent (Vector Laboratories) were added following the manufacturer's instructions. Secondary antibody only was used as negative control. Chromogenic reaction was developed with diaminobenzidine (Vector Laboratories); slides were counterstained using hematoxylin (Sigma Aldrich). ImageScope software (Leica Microsystems Inc.) was used to analyze images; staining intensity were converted to HScores using the formula [HScore = (% Positive) × (intensity) + 1].

RNA sequencing analysis

RNA sequencing analysis was carried out following our established conditions.[51] RNA was extracted from s.c. xenografts using a miRNeasy Mini Kit (Qiagen, No. 217004) according to the manufacturer's instructions; libraries were prepared with TruSeq Ribo Profile Mammalian Kit (Illumina, RPHMR12126) following manufacturer's instructions, and sequenced by BGI (a genomic sequencing center in Shenzhen, China) using the HiSeq 4000 system. RNA sequences were quantified by BGI (www.genomics.cn/en/navigation/show_navigation?nid=2657) and expressed as fragments per kilobase of exon per million fragments mapped (FPKM) according to the formula: $FPKM = 10^6C/(NL/10^3)$ with C being the number of fragments aligned to a specific gene, N representing the total number of fragments aligned, and L for the combined exon length of a gene. The mapping rates to human reference genome were 77% and 78% for two EV s.c. xenografts as well as 74% and 75% for two FAM84B s.c. xenografts; the analyses of DEGs were focused on human transcripts. DEGs in xenografts ($n = 2$) produced by DU145 FAM84B cells *versus* tumors ($n = 2$) generated from DU145 EV cells were determined using the Poisson distribution method by BGI.

Pathway enrichment analysis

Pathway enrichment analyses for FAM84B-associated DEGs were performed using the Reactome[52] packages in R Software.

Cutoff point estimation

Cutoff point of DEG expression to separate PC recurrence was estimated using Maximally Selected Rank Statistics (the *Maxstat* package) in R.

Establishing of a multigene panel predicting PC recurrence

The largest TCGA (The Cancer Genome Atlas) provisional dataset within the cBioPortal database[53,54] (www.cbioportal.org/index.do) contained 490 PCs with follow-up data; all tumors

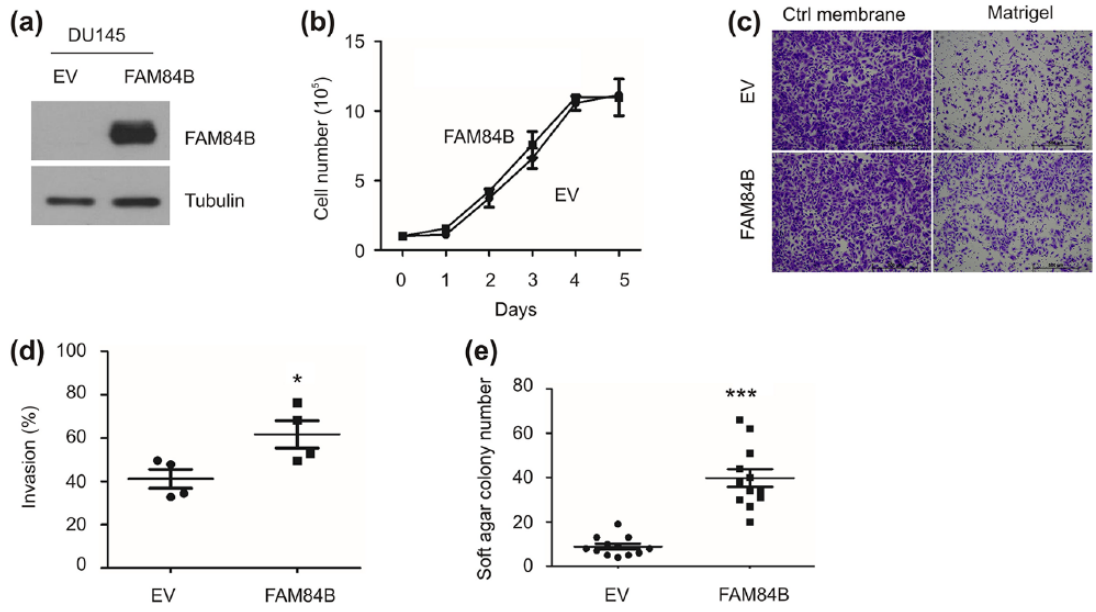

Figure 1. FAM84B increase DU145 cell invasion and growth in soft agar. (a) Western blot analysis of DU145 cells stably infected with an EV or FAM84B. (b) DU145 EV cells and DU145 FAM84B cells were analyzed for proliferation. The indicated cells were seeded in six-well plates at 10^5/well. Cell numbers were counted in triplicates; experiments were repeated three times; means ± SD are graphed. (c, d) DU145 EV and FAM84B cells were examined for invasion by Transwell plates using a control or Matrigel-coated membrane insert. Cells passing through the membranes were stained with crystal violet. Experiments were repeated four times. Typical images from a single repeat are shown (c); data are quantified; means ± SEM are graphed (d). *: $p < 0.05$ (two-tailed Student's *t* test) in comparison with DU145 EV cells. (e) DU145 EV and DU145 FAM84B cells were seeded in soft agar (10^4 cell/well, six-well plate). Colonies were imaged and counted. Experiments were repeated three times with multiple wells; the colony distribution and means ± SEM are graphed. ***: $p < 0.001$ (two-tailed Student's *t* test) in comparison with DU145 EV cells.
EV, empty vector; SD, standard deviation; SEM, standard error of the mean.

were profiled for mRNA expression using RNA sequencing. The dataset was used to select a gene signature predicting PC recurrence among 4976 DEGs using elastic-net logistic regression within the *glmnet* package in R with the mixing parameter α set at 0.2, 0.5, and 0.8 and cross validation set at 10-fold.

Statistical analysis

Kaplan–Meier survival curves and a log-rank test were performed using the R *survival* package, and tools provided by cBioPortal. Univariate and multivariate Cox regression analyses were carried out with the R *survival* package. Time-dependent receiver operating characteristic (tROC) analysis was used (the R *timeROC* package). A two-tailed Student's *t* test, two-way analysis of variance (ANOVA), and Benjamini–Hochberg post hoc test were performed. A value of $p < 0.05$ was considered statistically significant.

Results

FAM84B Overexpression promotes DU145 cell invasion and growth in soft agar

We recently showed an upregulation of FAM84B in DU145-derived PC stem-like cells and an association of FAM84B upregulation with PC progression.[45] To investigate whether FAM84B is functionally important in prostate tumorigenesis, we stably expressed an EV or FAM84B in DU145 cells [Figure 1(a)]; the respective pool populations of the EV and FAM84B stable lines were used. The overexpression was justified as the basal level of FAM84B expression was substantially lower in nonstem-like or monolayer DU145 cells in comparison with PC3 and LNCaP cells.[45] Based on three independent western blot analyses with α-tubulin as the loading control, FAM84B expression was 25-fold higher in DU145 FAM84B cells compared with DU145 EV cells ($p < 0.001$ by a two-tailed Student's *t*

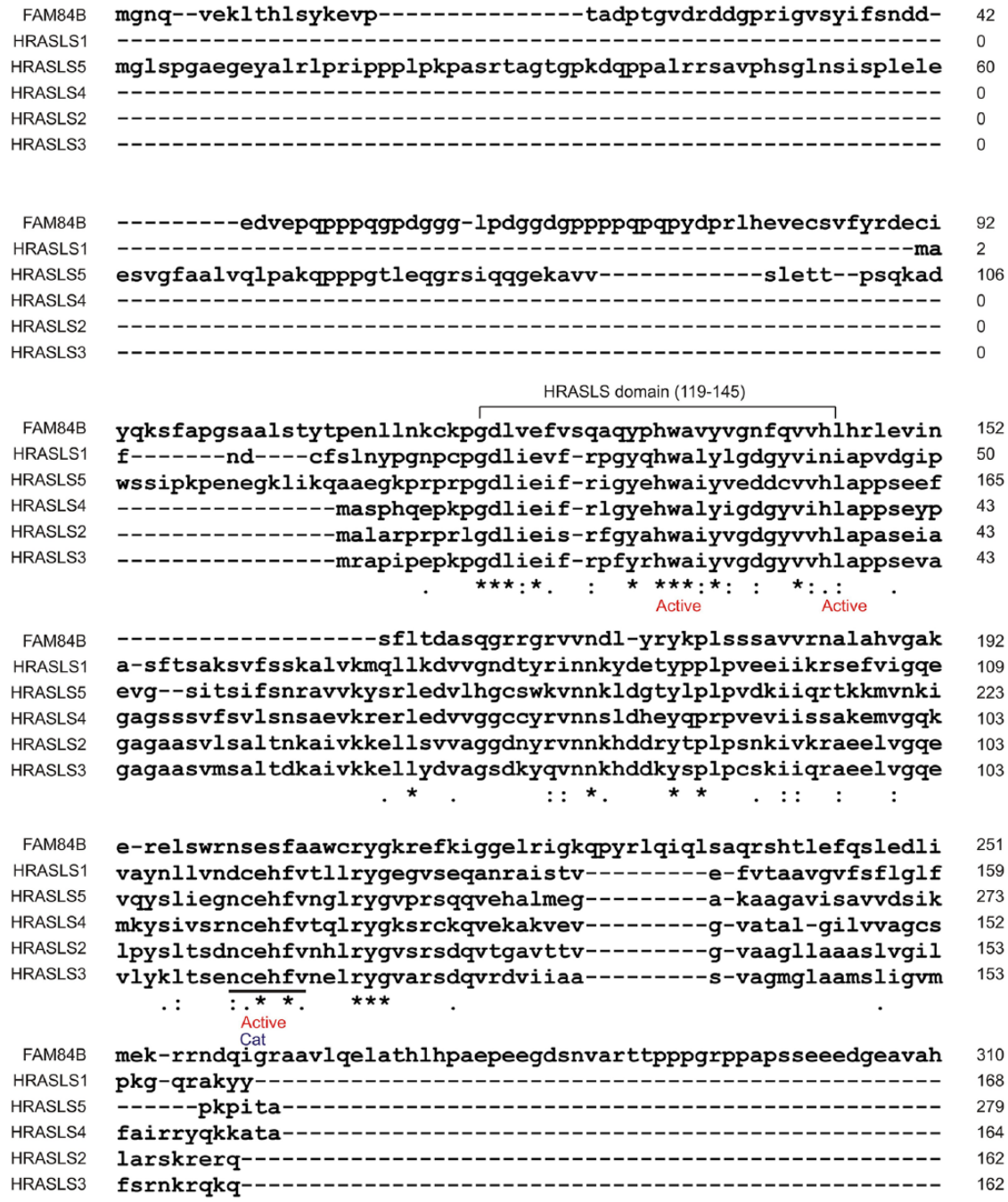

Figure 2. Multiple alignment of FAM84B with the HRASLS family members. The alignment of FAM84B with HRASLS1-5 was performed using CLUSTAL 2.1 Multiple Sequence Alignments (www.ebi.ac.uk/Tools/msa/clustalw2/). The three active residues (active) H23, H35, and C113 numbered according to HRASLS2 are indicated; the catalytic (Cat) residue C113 is also shown. The highly conserved residues NCEHFV among HRASLS1-5 are underlined. The FAM84B fragment encompassed residues 119–145 with the highest level of homology with HRASLS1-5 is indicated as 'HRASLS domain (119–145)'.
HRASLS, H-Ras-like suppressor; NCEHFV, amino acid residues of asparagine (N), cysteine (C), glutamic acid (E), histidine (H), phenylalanine(F), and valine (V).

test). Overexpression of FAM84B was without effects on DU145 cell proliferation [Figure 1(b); Figure S1], but elevated the cell's ability for invasion [Figure 1(c, d)] and colony formation in soft agar [Figure 1(e)]. Multiple attempts were made to knockdown FAM84B in DU145 cells without obvious success by using a pool of 3 FAM84B sh-RNA lentivirus (Santa

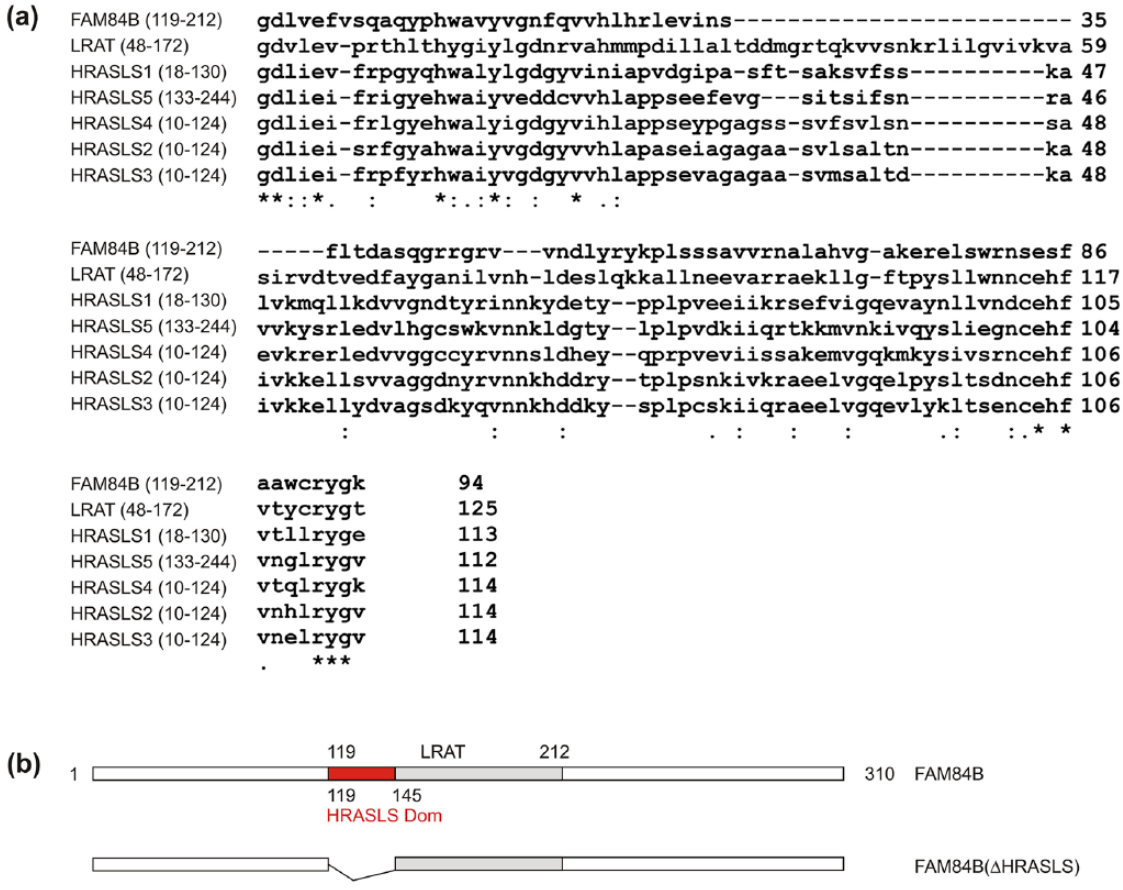

Figure 3. Alignment of the LRAT homologous domain in FAM84B and HRASLS1-5. (a) The LRAT domain from FAM84B, LRAT, and the HRASLS1-5 are aligned using CLUSTAL 2.1 Multiple Sequence Alignments. (b) Strategy used to construct the FAM84B (ΔHRASLS) deletion mutant.
LRAT, lecithin:retinal acyltransferase.

Cruz) that we have previously shown to be effective (data not shown); this lack of success might be in part attributable to the low level of endogenous FAM84B expression in DU145 cells.[45]

Characterization of FAM84B-derived oncogenic activities

With our unsuccessful attempt to knockdown FAM84B in DU145 cells, an alternative method was used to further examine the FAM84B-promoted processes of invasion and growth in soft agar *in vitro*. We first performed a structural analysis and observed similarities between FAM84B and the HRASLS family (Figure 2); a multiple alignment revealed a region in FAM84B marked with residues 119-212 that is conserved with a region in the members of HRASLS (Figure 2). Humans have five HRASLS members (HRASLS1-5), which all display activities suppressing H-Ras *in vitro*.[46] HRASLS1-5 are enzymes with phospholipase $A_{1/2}$ activities and O-acyltransferase activities.[46] The active site is formed by histidine 23 (H23), H35, and cysteine 113 (C113) numbered in HRASLS2 with C113 being the catalytic residue (Figure 2).[46,55] The catalytic triad is conserved among the five HRASLS except the H35 being functionally replaced by asparagine (N) in HRASLS1 (Figure 2).[46] In FAM84B, both H23 and H35 are conserved but not the catalytic residue C113 (Figure 2). As C113 is required for the enzymatic activities,[46] FAM84B is unlikely to possess either phospholipase $A_{1/2}$ activities or O-acyltransferase enzymatic activities.

We further noticed that the conserved FAM84B region (residues 119-212) is actually the LRAT homologous domain [Figure 3(a)]. The LRAT

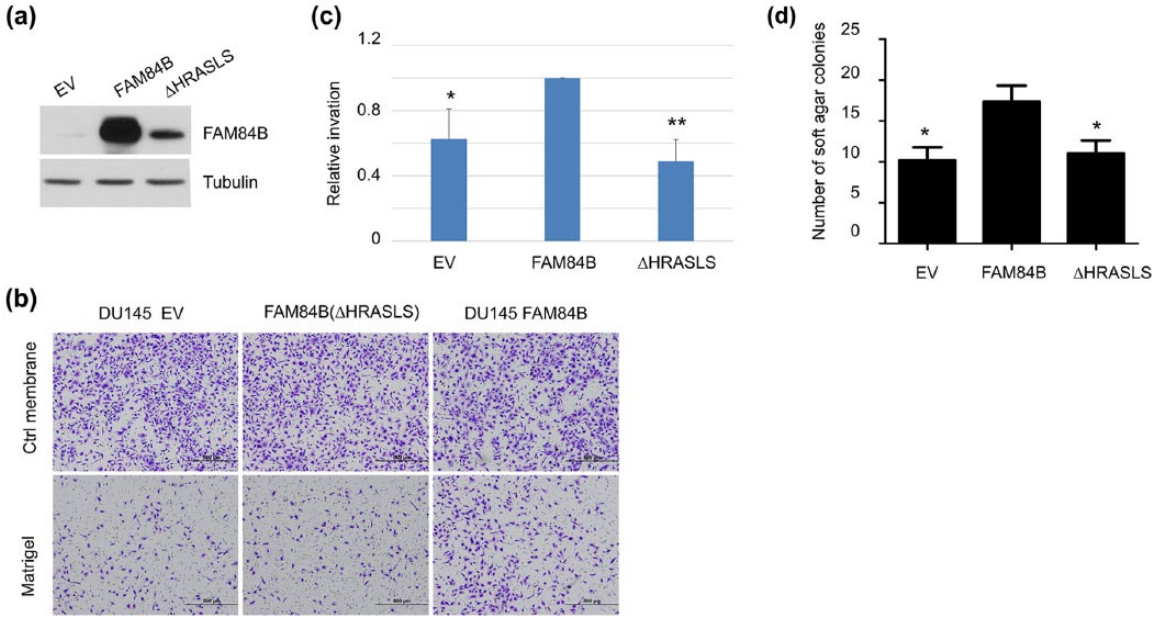

Figure 4. FAM84B (ΔHRASLS) is incapable of increasing DU145 cell invasion and growth in soft agar. (a) DU145 cells were stably expressed with EV, FAM84B or FAM84B (ΔHRASLS). (b–d) DU145 cells expressing EV, FAM84B, or FAM84B (ΔHRASLS) were analyzed for cell invasion (b, c) and growth in soft agar (d). Experiments were repeated three times. Means ± SEM are graphed. *: $p < 0.05$ and **: $p < 0.01$ (two-tailed Student's *t* test) in comparison with DU145 FAM84B cells.
EV, empty vector; SEM, standard error of the mean.

domain is a typical motif of the HRASLS family[46]; this domain is also aligned among FAM84B, LRAT, and HRASLS1-5 [Figure 3(a)]. A subregion exists in this LRAT domain, bordered by the residues 119–145 in FAM84B, which is highly conserved between FAM84B and the HRASLS family (Figure 2). We tentatively named this motif the HRASLS domain or HRASLS (Figure 2).

To investigate whether the HRASLS domain plays a role in FAM84B-derived enhancement of cell invasion and growth in soft agar, a mutant with this motif deleted was constructed [Figure 3(b)], and was stably expressed in DU145 cells [Figure 4(a)]. Expression of FAM84B (ΔHRASLS) did not affect cell proliferation [Figure S2(a, b)] and was not able to enhance cell invasion [Figure 4(b); $p = 0.8$] and growth in soft agar compared with DU145 EV cells [Figure S2(c)]. Nonetheless, in comparison with DU145 FAM84B cells, DU145 FAM84B (ΔHRASLS) cells displayed a reduction in invasion and growth in soft agar [Figure 4(b–d)]. Collectively, the above observations support that the HRASLS domain makes a major contribution to FAM84B's activity in promoting DU145 cell invasion and growth in soft agar.

Evidence suggests an intramolecular interaction between FAM84B molecules

We have attempted to examine whether an intramolecular interaction exists for FAM84B, which may suggest a potential mechanism for FAM84B's actions in PC. For this purpose, we have taken advantage of the FAM84B (ΔHRASLS) mutant and FAM84B tagged with an HA and FLAG epitope, respectively. When both were transiently expressed in 293T cells, immunoprecipitation of one led to co-precipitation of another [Figure 5(a)]. When DU145 cells were transiently co-transfected with both, the mutant and wild type FAM84B can be expressed in the cytosol and nucleus; a co-localization can be clearly demonstrated [Figure 5(b)]. However, the expression patterns of FAM84B and FAM84B(ΔHRASLS) are not identical [Figure 5(b)], suggesting that the observed co-localization was unlikely due to overexpression. Collectively, evidence supports an intramolecular interaction between the

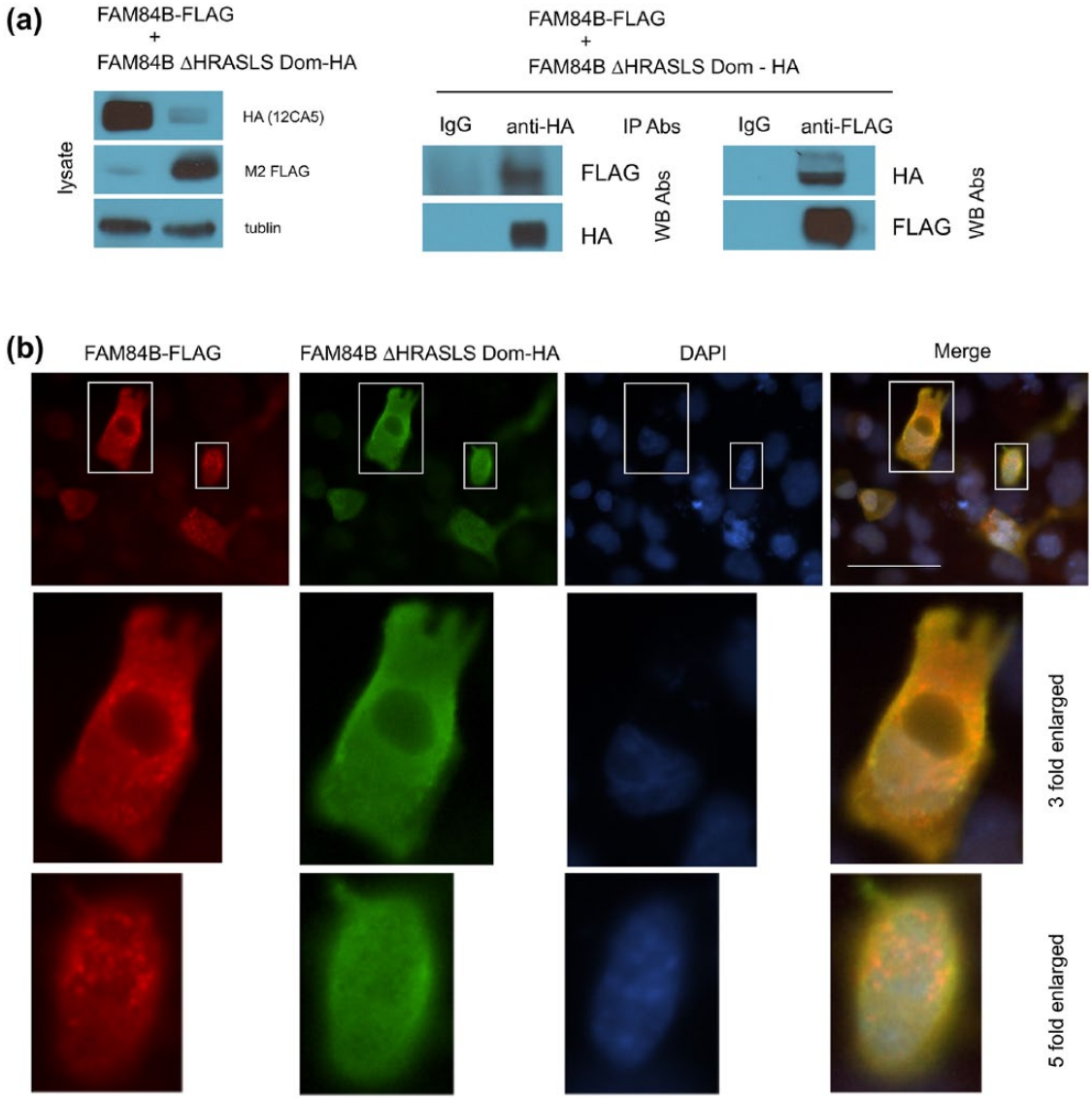

Figure 5. Intramolecular interaction of FAM84B. (a) 293T cells were transiently transfected with FLAG-tagged FAM84B and HA-tagged FAM84B (ΔHRASLS). Cell lysates were immunoprecipitated with either anti-HA (middle panel) or anti-FLAG (right panel), followed by WB analysis for the indicated Abs. 1% of cell lysates was examined for transgene expression (left panel). (b) DU145 cells were transiently transfected with FLAG-tagged FAM84B and HA-tagged FAM84B (ΔHRASLS); dual immunofluorescence staining for FAM84B and FAM84B (ΔHRASLS) was performed using anti-FLAG and anti-HA antibodies respectively. Nuclei were counterstained with DAPI. Merge images are included. Scale bar represents 100 μM. Experiments were repeated three times; typical images from a single repeat are shown. The marked regions are enlarged three or five-fold and placed beneath the individual panels.
Abs, antibodies; DAPI, 4′,6-diamidino-2-phenylindole; FLAG, a commonly used polypeptide epitope tag; HA, a tag epitope derived from hemagglutinin; WB, western blot.

FAM84B molecules and the interaction is likely independent of the HRASLS motif.

FAM84B upregulation enhances xenograft tumor formation in vivo

The observed enhancement of DU145 cell invasion and growth in soft agar indicates that FAM84B promotes prostate tumorigenesis. To examine this possibility, we subcutaneously implanted DU145 EV cells and DU145 FAM84B cells in NOD/SCID mice ($n = 5$ per group). As expected, a high level of FAM84B expression was shown in xenografts produced by DU145 FAM84B cells at both the protein and mRNA levels [Figure 6(a, b); Figure S3]. DU145 FAM84B cell-generated

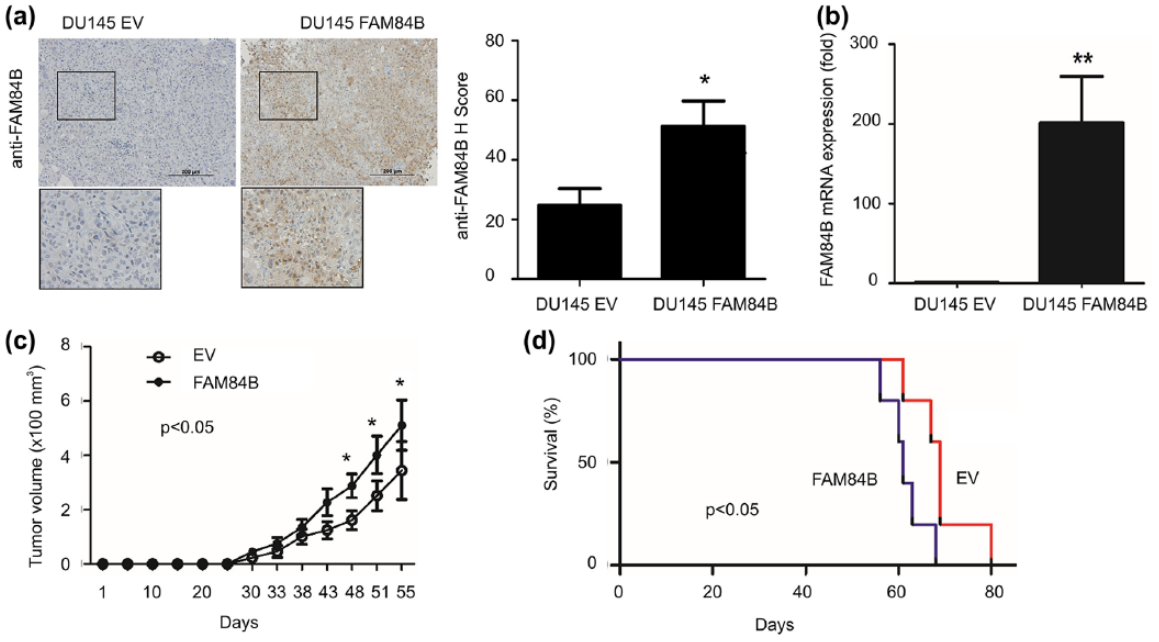

Figure 6. FAM84B promotes xenograft growth. DU145 EV and DU145 FAM84B cells were s.c. implanted into NOD/SCID mice (5 mice per group). (a) IHC staining for FAM84B in the indicated xenografts ($n = 5$ for each tumor type); typical images with two-fold enlargement of the marked regions are shown (left panel); staining was quantified using H scores; means ± SEM are graphed. *: $p < 0.05$ (two-tailed Student's t test) in comparison with DU145 EV xenografts. (b) Real-time PCR analysis of FAM84B mRNA expression in the indicated tumors ($n = 5$). FAM84B mRNA expression was normalized to the respective actin mRNA. Relative FAM84B mRNA expression is graphed. **: $p < 0.01$ by a two-tailed Student's t test. (c) Volumes (means ± SEM) for the indicated tumors. Statistical analysis was performed using two-way ANOVA ($p < 0.05$). A Benjamini post hoc test was also carried out; *: $p < 0.05$. (d) Kaplan–Meier survival analysis of the kinetics reaching the volume endpoint (≥1000 mm^3); statistical analysis was performed using a log-rank test.
ANOVA, analysis of variance; IHC, immunohistochemistry; PCR, polymerase chain reaction; s.c., subcutaneously; SEM, standard error of the mean.

xenografts grew significantly faster than DU145 EV cell-generated tumors [Figure 6(c)] and reached the volume endpoint (≥1000 mm^3) earlier [Figure 6(d)]. Taken together, these observations revealed that FAM84B possesses activities in promoting xenograft growth, which is in accordance with the previously reported association of FAM84B upregulation with PC.[45]

FAM84B upregulation facilitates PC metastasis

To examine a potential role of FAM84B in facilitating PC metastasis, we injected DU145 EV or DU145 FAM84B cells *via* the tail vein into NOD/SCID mice ($n = 6$ and $n = 10$ for the former and latter group respectively). The kinetics for animals reaching the endpoint of weight drop ≥10% was analyzed. In comparison with mice injected with DU145 EV cells, animals receiving DU145 FAM84B cells reached the endpoint more rapidly [Figure 7(a)]. As expected, all animals showed lung metastasis (Figure S4). As well, tumors derived from DU145 FAM84B cells expressed a higher level of FAM84B compared with tumors produced by DU145 EV cells [Figure 7(b, c)].

AKT (protein kinase B) activation plays an important role in PC metastasis.[56] Consistent with this knowledge, we were able to show an elevation of AKT activation in DU145 FAM84B cell-produced lung metastases compared with DU145 EV cell-derived metastases [Figure 8(a)]. One of AKT's most well-studied functions is its pro-survival role,[57] suggesting a survival advantage in lung metastases produced by DU145 FAM84B cells. To further investigate this possibility, we examined the pro-apoptotic protein BAD in the above lung metastases and observed a significant reduction of BAD in DU145 FAM84B cell-derived lung metastases [Figure 8(b)]. As we did not observed an elevation in AKT activation in DU145 FAM84B cells compared with DU145 EV cells *in vitro*, these alterations were specific in metastasis, and likely result of the process of

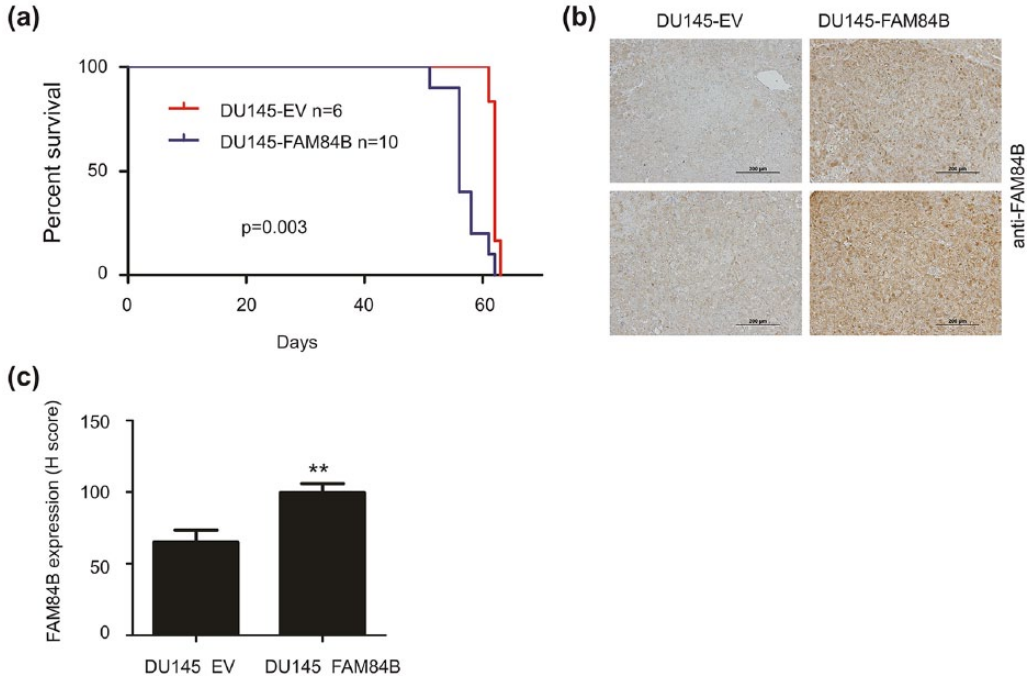

Figure 7. FAM84B enhances PC metastasis. DU145 EV ($n = 6$) and DU145 FAM84B ($n = 10$) cells were injected into NOD/SCID mice through the tail vein. (a) Mice bearing the indicated metastasis were analyzed for durations reaching an endpoint (weight drops ⩾10%) using a Kaplan–Meier survival curve and log-rank test. (b, c) Lung metastasis was examined for FAM84B expression using IHC; typical images for two tumors of each type are shown (b); quantification of FAM84B expression in all tumors is graphed (c). **: $p < 0.01$ by a two-tailed Student's *t* test in comparison with DU145 EV metastasis.
EV, empty vector; IHC, immunohistochemistry; PC, prostate cancer.

tumor growth *in vivo*. Collectively, these observations indicate a potential mechanism by which FAM84B facilitates PC growth in the lung.

FAM84B activates a network in vivo

The role of FAM84B overexpression in promoting PC tumorigenesis is in line with the low level of FAM84B protein expression in prostate among other human tissues (Figure S5). To investigate the mechanisms whereby FAM84B enhances xenograft growth, we have profiled the transcriptome of tumors produced by DU145 EV cells ($n = 2$) or DU145 FAM84B cells ($n = 2$). The probability of DEGs for the setting of two tumor types (groups) and two tumors per group were determined by the Poisson distribution statistical module; the analyses were performed by BGI (see Methods for details) using an algorithm developed by BGI. In reference to the significant elevation of FAM84B mRNA in DU145 FAM84B cell-produced xenografts compared with DU145 EV cell-derived tumors [Figure 6(b)], DEGs were defined using the probability (0.319383) which selects FAM84B as one of the DEGs, that is DEGs were selected by their probability ⩾0.319383 (Table S1); a total of 4976 DEGs were found (Table S1).

We then analyzed pathways that were enriched by these 4976 DEGs. Using the Reactome package in R, 51 pathways were found to be enriched (Table S2). Enrichment map revealed that these pathways were clustered in four major processes: the Golgi-to-ER process, cell cycle checkpoint, mitochondrial events, and protein translation (Figure 9). In line with this enrichment map analysis, the top 12 enriched pathways were within these processes [Figure 10(a, b)]. As expected, the alterations among the top five pathways were largely overlapped; these five pathways are connected to the enriched pathway of cellular response to stress (Figure S6). Additionally, the directionality (upregulation and downregulation) of the component DEGs in these pathways were also illustrated (Figure S6).

We further analyzed pathway enrichment using Gene Set Enrichment Analysis (GSEA). Consistent with the above analyses, significant

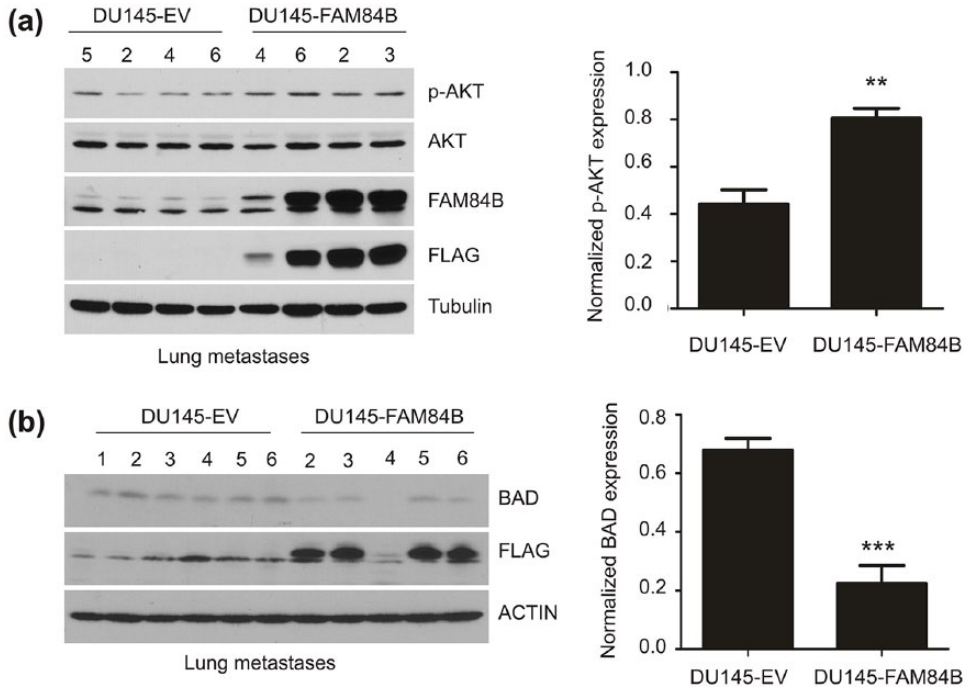

Figure 8. Elevation in AKT activation and downregulation of BAD expression in lung metastases produced by DU145 FAM84B cells. (a) DU145 EV lung metastases #5, #2, #4, and #6 and the indicated DU145 FAM84B metastases were examined for AKT activation (phosphorylation at serine 473, p-AKT), AKT, FAM84B (*via* detection of endogenous FAM84B or ectopic FAM84B/FLAG), and tubulin expression. Western blot images (left panel) and normalized p-AKT (p-AKT/AKT) levels (right panel) are provided. (b) Western blot images for the indicated proteins in the lung metastases of either DU145 EV or DU145 FAM84B (left panel). BAD expressions in DU145 EV metastasis ($n = 6$) and DU145 FAM84B ($n = 5$) were normalized to the respective actin; means ± SEM are graphed. $^{**}p < 0.01$ and $^{**}p < 0.001$ by a two-tailed Student's *t* test in comparison with DU145 EV metastasis. Experiments in (a) setting was also performed in (b) setting; essentially the same results were obtained.
AKT, protein kinase B; EV, empty vector; SEM, standard error of the mean.

downregulation of the gene set regulating cellular responses to stress in DU145 FAM84B cell-generated xenografts was observed (Figure 11; R-HSA-2262752). Downregulation of gene sets functioning in G2/M checkpoints and cell cycle checkpoints were also detected (Figure 11; R-HSA-69481 and R-HSA-69620). These reductions would be expected to facilitate xenograft growth, which is supported by the data presented in Figure 6. Reduction in the citric acid cycle (CTA) and respiratory electron transport (Figure 11; R-HSA-1428517) is supported with the enriched pathways regulating mitochondrial events (Figure 9). In DU145 FAM84B cell-derived tumors, the ubiquitination-involved processes were altered (Figure 11; R-HSA-5688426). Tumorigenesis and tumor progression are associated with alterations in DNA methylation and global hypomethylation[58]; of note, xenografts produced by DU145 FAM84B cells exhibited a reduction in the gene set regulating DNA methylation in comparison with tumors derived from DU145 EV cells (Figure 11; R-HSA-5334118).

Building a multigene signature predicting PC recurrence

The pathway enrichment analyses above suggests an association of the 4976 DEGs with PC progression; among which BCR was found to significantly increase the risk of PC metastasis.[10] We thus analyzed a potential association of the 4976 DEGs with BCR. TCGA provisional genomic dataset of PC within the cBioPortal database contains 499 tissue samples with follow-up data and mRNA profiles from RNA sequencing. From this cohort, 490 PC tissues/patients were used for model building. Following our previously established conditions,[59–61] the downregulated DEGs ($n = 2471$) were analyzed at $1.5\times$ SD (standard deviation), $-1.5\times$ SD below a reference population mean, and the upregulated DEGs ($n = 2505$)

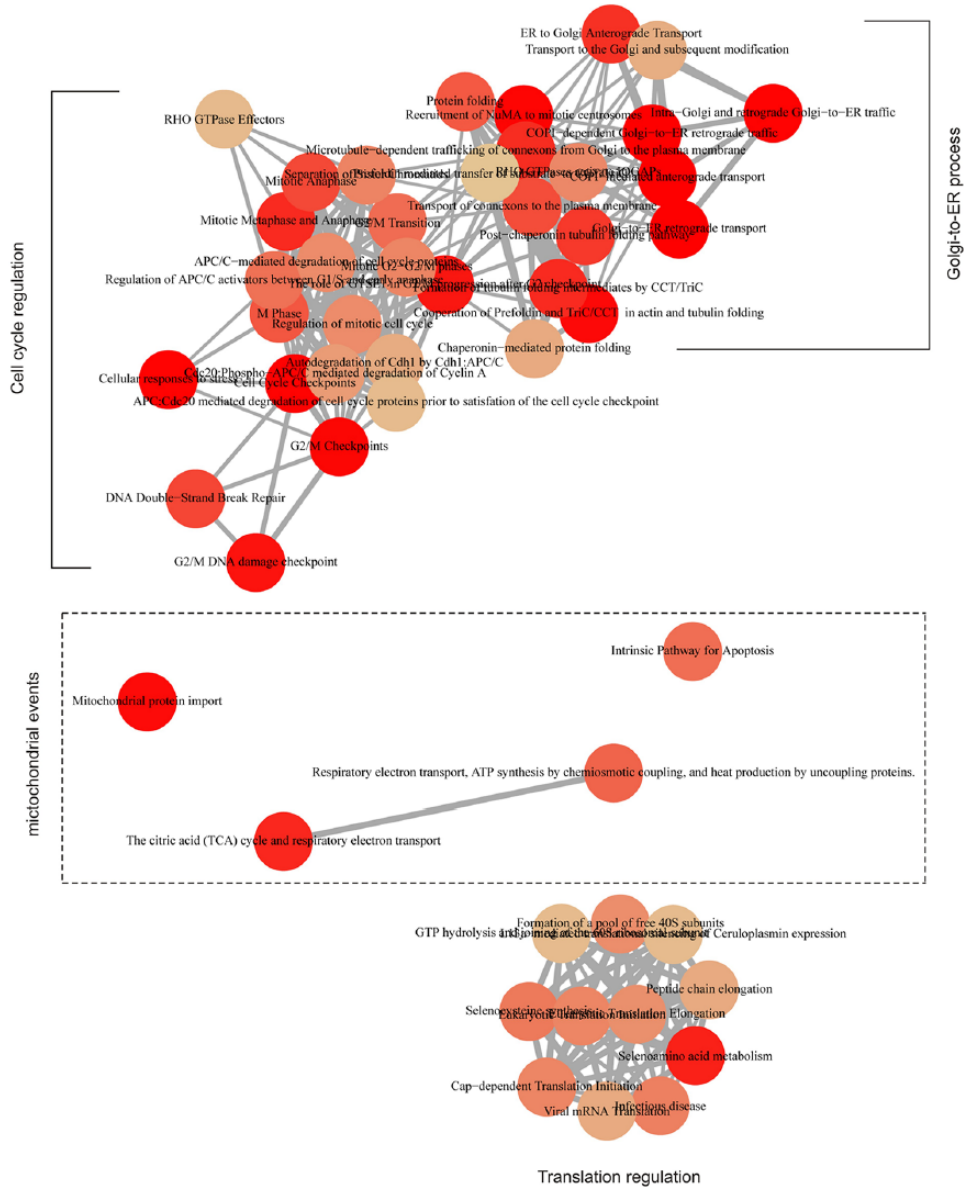

Figure 9. Enrichment mapping of the pathways enriched in DU145 FAM84B xenografts. Pathway enrichment analysis was performed using Reactome in R (see Table S2 for details of enriched pathways); each circular symbol represents individual pathways. The connections among these pathways are shown. The presentation was generated using Reactome in R.

were evaluated at 2 × SD above a reference population mean [Figure 12(a)]. All tumors (n = 490) were assigned a binary code of '1' if downregulated DEGs were expressed $<-1.5 \times$ SD, or upregulated DEGs were expressed $>2 \times$ SD; otherwise tumors were assigned '0'. This reorganized population was then used to analyze the impact of DEGs (n = 4976) on PC recurrence with elastic-net regression within the R *glmnet* package with 10-fold cross validation. To enhance the selection of highly correlated covariate as a group, the mixing parameter α was set at 0.2, 0.5 and 0.8; for each mixing parameter, six independent selections were performed. The core DEGs present in all selections plus unique DEGs with a total of 51 genes were initially selected. We then used a different approach to reanalyze these 51 DEGs; cutoff points to separate PC recurrence were estimated using Maximally Selected Rank Statistics in R. Each tumor was then given a

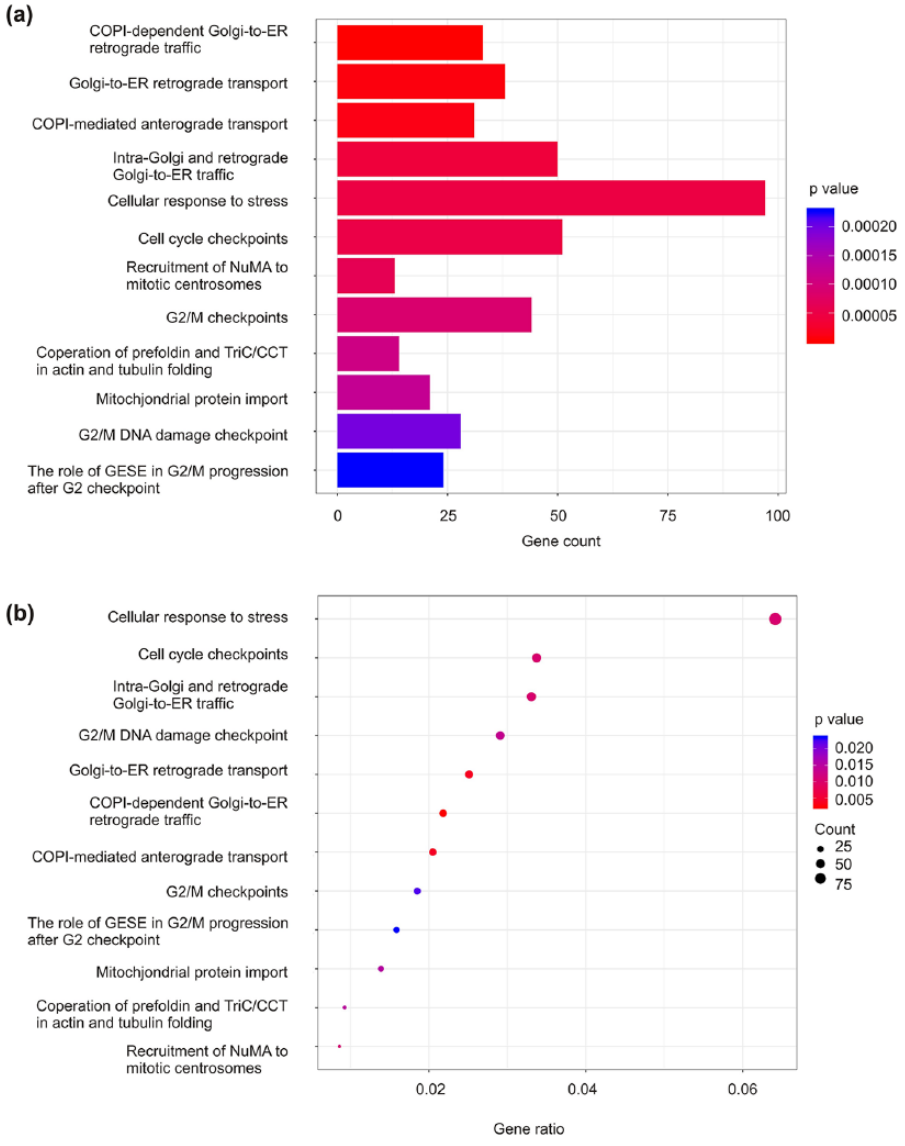

Figure 10. The top 12 pathway enriched by DEGs relative to FAM84B overexpression. The 4976 DEGs (Table S1) were examined for pathway enrichment with the Reacome package in R. The top 12 pathways are included for the number of genes (a) and the gene ratio involved (b).
DEG, differentially expressed gene.

binary code '0' or '1' accordingly; the individual component gene was analyzed for an association with PC recurrence by univariate Cox proportional hazards (PH) regression analysis; the PH assumption were confirmed. All component genes ($n = 27$) with a significant association with PC recurrence were selected to build SigFAM (Table 1).

To analyze SigFAM's potential in stratification of the risk of PC recurrence, SigFAM scores were calculated for individual tumors using the formula $\Sigma(f_i)_n$ (f_i: Cox coefficient of $gene_i$, $n = 27$). The scores discriminate PC recurrence with time-dependent area under the curve (tAUC) values of 0.824 at 11.6 month (0.824/11.6 M), 0.792/22.3 M, 0.808/32.1 M, and 0.793/48.4 M [Figure 12(b)]. The cutoff point of SigFAM was then estimated (Figure S7); SigFAM is robustly associated with a reduction in disease-free survival (DFS) in PC [Figure 12(c)] with sensitivity, specificity, and positive predictive value (PPV) being 63.7%, 79.9%, and 42% respectively.

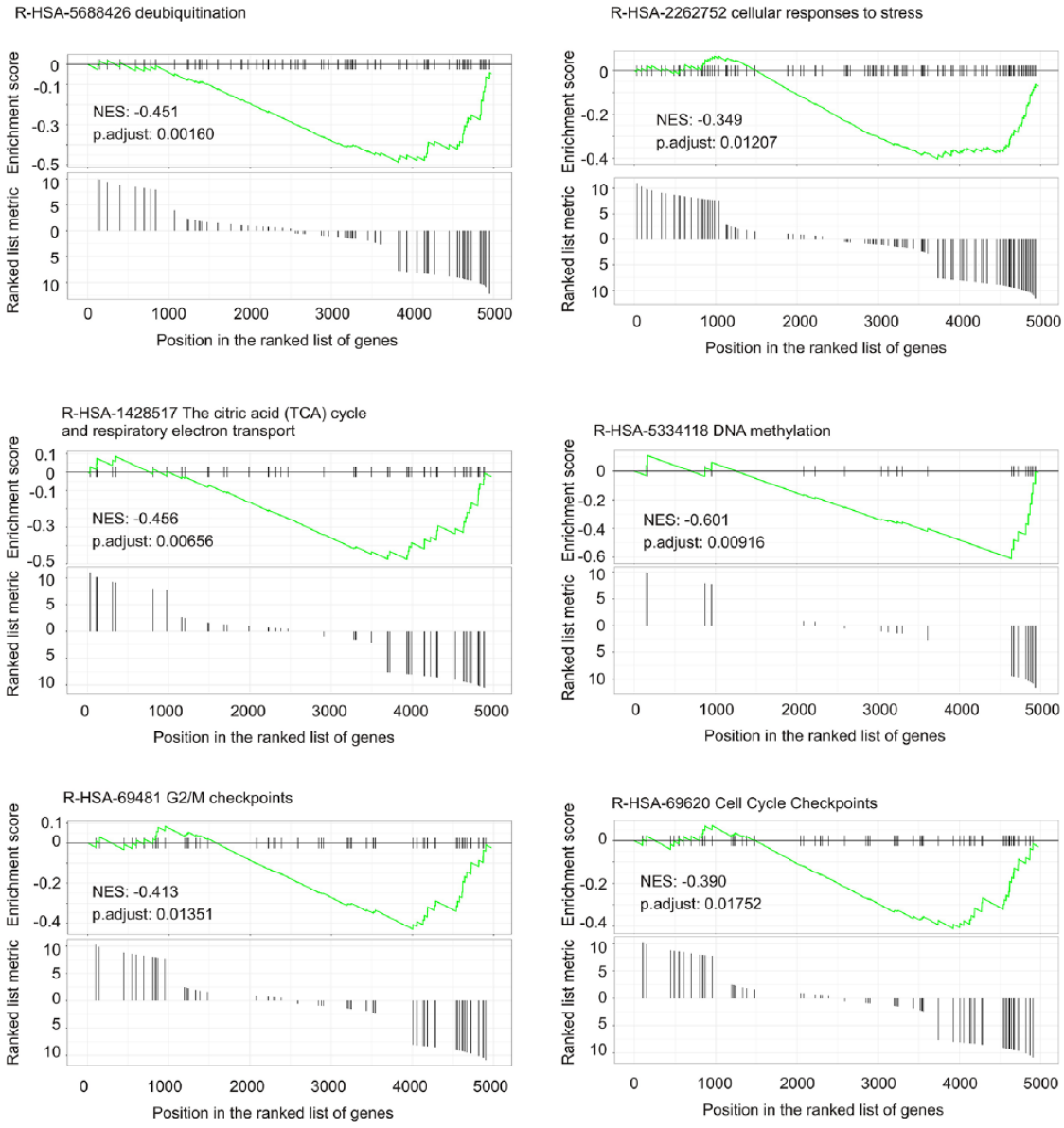

Figure 11. DU145 FAM84B cell-produced xenografts show downregulation in the indicated gene sets. GSEA was performed using Reacome in R.
GSEA, Gene Set Enrichment Analysis; NES: normalized enrichment score; *p*.adjust: adjusted *p* value.

The quartile 1 (Q1), median, and Q3 scores of SigFAM scores separate high and low risk group of PC recurrence with a range of sensitivity and specificity: 96.7% and 30.1% for Q1 [Figure 12(d)], 81.3% and 57.1% for Median [Figure 12(e)], and 54.9% and 81.7% for Q3 [Figure 12(f)]. SigFAM can thus stratify PC recurrence with a high level of sensitivity (96.7%) and specificity (81.7%) through the combinational use of Q1, median, Q3, and cutoff point.

We evaluated the effectiveness of SigFAM in the stratification of BCR in comparison with the multigene signature Prolaris (cell cycle progression; CCP),[62] a commercially available gene set used to predict BCR following prostatectomy.[62,63] We have previously shown that the 31-gene CCP classified PC recurrence using the TCGA provisional (n = 490) dataset (cBioPortal) at a sensitivity of 27.47% (25/91), specificity of 85.96% (343/399), PPV of 30.86% (25/81), median

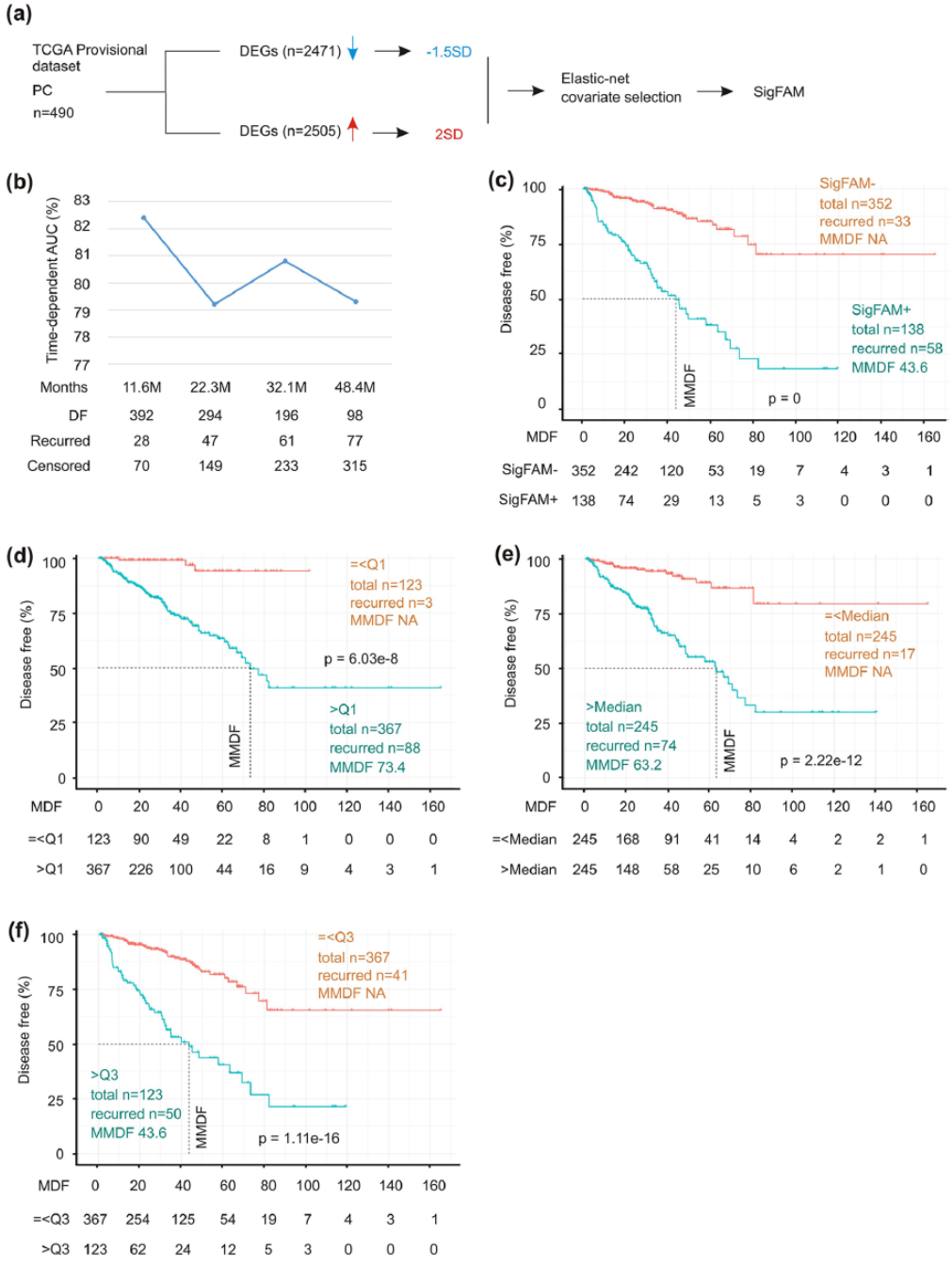

Figure 12. SigFAM effectively stratifies PCs with elevated risk of recurrence. (a) The outline to build a multigene panel. TCGA provisional PC dataset (cBioPortal) was assigned according to the expression of downregulated DEGs and upregulated DEGs at the indicated levels; −1.5 × SD and 2 × SD indicate expression below and above a reference population mean. The reorganized cohort was subsequently examined for impact of these DEGs on PC recurrence (DFS) using the elastic-net regression (R *glmnet* package); the 27-gene SigFAM was the result. (b) PCs ($n = 490$) of the TCGA cohort were scored for SigFAM, which was analyzed for discrimination of PC recurrence using tROC. tAUC together with the status of PC recurrence are graphed. (c) SigFAM scores were estimated for a cutoff point to separate PC recurrence (see Figure S7), followed by analyzing its stratification of the high-risk group of PC recurrence. Numbers of patient at risk during the indicated follow-up period are given. (d–f) SigFAM was analyzed to separate PCs at risk of recurrence using its Q1 score (d), Median score (e), and Q3 score (f). Kaplan–Meier curve and log-rank test were performed with the Survival package in R.

AUC, area under the curve; DEG, differentially expressed gene; DFS, disease-free survival; MDF, months disease free; MMDF, median months disease free; NA, MMDF was not reached; PC, prostate cancer; SD, standard deviation; tAUC, AUC at the indicated time; TCGA, The Cancer Genome Atlas; tROC, time-dependent receiver operating characteristic.

Table 1. Association of the component genes of SigFAM with PC recurrence[a].

Genes	Coef[b]	HR[c]	95% CI[d]	*p* value
UFM1[e,g]	0.9031	2.467	1.625–3.746	2.24e^{-5}***
ARPC2[f]	0.7107	2.035	1.347–3.705	0.000733***
FAAP24[f]	0.5632	1.756	1.086–2.841	0.0218*
PPA2[f]	0.555	1.742	1.131–2.682	0.0117*
CHEK2[f,g]	0.8279	2.288	1.513–3.462	8.9e^{-5}***
CRIP2[f,g]	0.9807	2.479	1.579–3.891	7.97e^{-5}***
RELT[f,g]	0.9266	2.516	1.619–3.908	4.05e^{-5}***
RAB32[f]	0.5767	1.78	1.166–2.718	0.00753**
CLBA1[f]	0.6914	1.996	1.3–3.067	0.00159**
KIF9[f]	0.6163	1.852	1.227–2.796	0.00335**
CCDC137[f]	0.6558	1.927	1.248–2.975	0.0031**
TICRR[f,g]	1.2187	3.383	2.192–5.22	3.64e^{-8}***
VWA5B2[f,g]	1.0498	2.857	1.889–4.322	6.68e^{-7}***
PIM1[f]	0.5327	1.704	1.068–2.717	0.0253*
FOXM1[f,g]	1.1228	3.073	2.035–4.461	9.27e^{-8}***
LRWD1[f]	0.6928	1.999	1.313–3.043	0.00123**
SYK[f]	0.7098	2.033	1.345–3.074	0.000762***
SCML2[f]	0.4789	1.614	1.065–2.447	0.024*
TRIM65[f,g]	1.1559	3.177	2.191–4.805	4.33e^{-8}***
ADCY7[f]	0.5792	1.785	1.163–2.739	0.00806**
ASF1B[f,g]	1.0683	2.911	1.907–4.442	7.35e^{-8}***
PUS7[f]	0.5342	1.706	1.054–2.761	0.0297*
BGN[f]	0.7067	2.027	1.335–3.978	0.000911***
ITGA11[f]	0.7021	2.018	1.337–3.047	0.000837***
RAD54L[f,g]	1.2258	3.407	2.252–5.155	6.52e^{-9}***
KCTD7[f]	0.6187	1.856	1.17–2.947	0.00869**
TIAM2[f]	0.5697	1.768	1.167–2.677	0.00713**

[a]Univariate Cox analysis was performed using The Cancer Genome Atlas provisional cohort ($n = 490$);
[b]Cox coefficient;
[c]hazard ratio;
[d]confidence interval;
[e]downregulated gene;
[f]upregulated genes;
[g]these genes form SigFAM1.
*$p < 0.05$; **$p < 0.01$; ***$p < 0.001$.
CI, confidence interval; PC, prostate cancer.

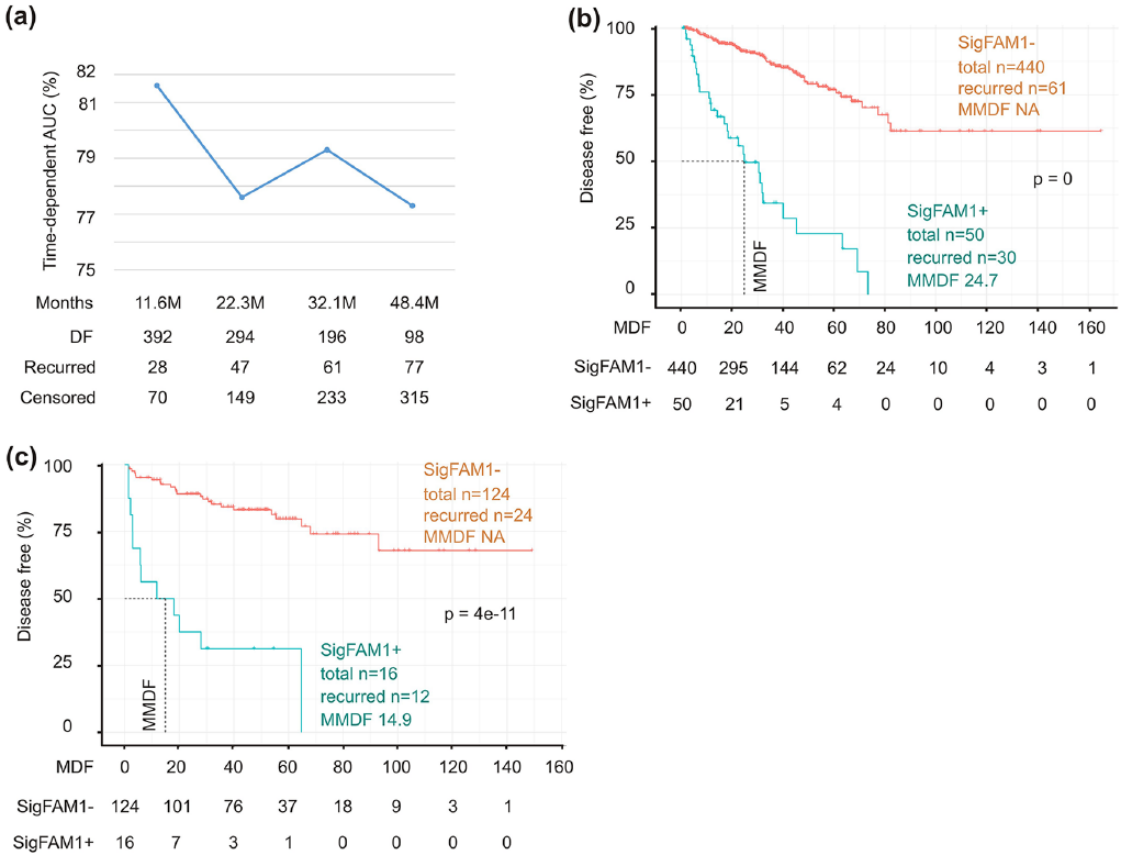

Figure 13. SigFAM1 is dramatically associated with a reduction in DFS. (a) Analysis of the performance of SigFAM1 in discriminating PC recurrence in the TCGA cohort. (b) Analysis of SigFAM1 in stratification of PCs at risk of recurrence in the TCGA cohort. (c) SigFAM1 is significantly associated with a reduction in DFS in the MSKCC dataset.
DFS, disease-free survival; MSKCC, Memorial Sloan Kettering Cancer Center; TCGA, The Cancer Genome Atlas.

months disease free (MMDF) at 66.89 months, and $p = 1.34e^{-4}$.[59] In comparison, SigFAM achieved sensitivity of 63.7%, specificity of 79.9%, PPV of 42%, MMDF at 43.6 months, and $p = 0$ [Figure 12(c)]. However, the CCP was analyzed using SD-based alterations here, while it was a real-time PCR-based assay in the clinic. It is likely that its predictive potential is underestimated in our system. Nonetheless, this analysis indicates that SigFAM should display comparable effectiveness as CCP in stratification of PC recurrence.

Characterization and validation of SigFAM

We noticed a subgroup of the SigFAM component genes that separate the high-risk population of PC recurrence with p value $\leqslant 8.9e^{-5}$, including UFM1, CHEK2, CRIP2, RELT, TICRR, VWA5B2, FOXM1, TRIM65, ASF1B, and RAD54L (Table 1). These genes were grouped into a sub-signature SigFAM1; its scores discriminate PC recurrence with tAUC 0.816 at 11.6 months, 0.776 at 22.3 months, 0.793 at 32.1 months, and 0.773 at 48.4 months [Figure 13(a)]. Using the cutoff point, SigFAM1 robustly stratifies PCs at risk of recurrence [Figure 13(b)]. SigFAM1 is more effective in separating early recurrence with MMDF at 24.7 [Figure 13(b)] in comparison with the MMDF at 43.6 for SigFAM [Figure 12(c)]. While SigFAM classifies the risk of PC recurrence with sensitivity 63.7%, specificity 79.9%, and PPV 42%, SigFAM1 stratifies PC recurrence risk at sensitivity 33%, specificity 95%, and PPV 60%. It thus may be optimal to combine SigFAM1 and SigFAM in the evaluation of early recurrence to achieve sensitivity, specificity, and PPV at 63.7%, 95%, and 60% respectively.

As SigFAM1 forms the core of SigFAM, we validated its biomarker value of PC recurrence using

Table 2. Univariate analysis of the SigFAM component genes in MSKCC.

Genes	Coefficient	HR	95% CI	*p* value
UFM1[a]	1.4736	4.356	2.1–9.072	7.87e^{-5}***
CHEK2[a]	0.9352	2.548	1.192–5.445	0.0158*
CRIP2[a]	0.8026	2.231	1.156–4.308	0.0168*
RELT[a]	0.9892	2.672	1.364–5.235	0.00417**
TICRR[a]	1.2702	3.562	1.816–6.983	0.000218***
VWA5B2[a]	1.0192	2.771	1.434–5.356	0.00244**
FOXM1[a]	1.9521	7.043	3.51–14.13	3.96e^{-8}***
TRIM65[a]	0.8935	2.444	1.263–4.729	0.00798**
ASF1B[a]	1.6868	5.402	2.659–10.98	3.11e^{-6}***
RAD54L[a]	1.0773	2.937	1.516–5.687	0.0014**
FAAP24	1.4199	4.137	2.056–8.322	6.87e^{-5}***
PPA2	0.9686	2.634	1.334–5.204	0.00529**
RAB32	1.2092	3.351	1.394–8.054	0.00688**
CLBA1	1.461	4.311	1.792–10.37	0.00111**
KIF9	1.1917	3.293	1.546–7.015	0.00201**
CCDC137	0.999	2.716	1.374–5.367	0.00405**
LRWD1	1.5298	4.617	2.144–9.942	9.25e^{-5}***
SYK	1.0848	2.959	1.496–5.851	0.00181**
SCML2	1.1178	3.058	1.391–6.722	0.00541**
ADCY7	1.4267	4.165	2.042–8.495	8.74e^{-5}***
BGN	1.4616	4.313	1.882–9.883	0.000551***
ITGA11	1.2749	3.578	1.858–6.981	0.000137***
TIAM2	1.152	3.163	1.615–6.196	0.000787***

[a]the component genes of SigFAM1.
*$p < 0.05$; **$p < 0.01$; ***$p < 0.001$.
CI, confidence interval; HR, hazard ratio.

an independent cohort. The Memorial Sloan Kettering Cancer Center (MSKCC)[64] PC dataset within cBioPortal has 140 patients/primary tumors with a follow-up period up to 140 months and were profiled for mRNA expression using DNA microarray (cBioPortal). Following our system as described above, we analyzed the component genes of SigFAM1 for associations with PC recurrence using their cut-off points. Univariate Cox analysis revealed that they all individually predicted PC recurrence (Table 2). Similar to the situation observed in the TCGA provisional cohort [Figure 13(b)], SigFAM1 displays specific effectiveness in the stratification of early recurrence in the MSKCC cohort [Figure 13(c)].

We also analyzed the biomarker value of SigFAM using the MSKCC cohort. Following the same system as described above, we showed that 23 out

of the 27 SigFAM component genes possessed predictive value towards PC recurrence in the MSKCC population (Table 2). Using these 23 genes, SigFAM effectively discriminates the high-risk group of PC recurrence with tAUC 85.4% at 18.4 months [Figure S8(a)]; its cutoff point powerfully stratifies PCs at risk of recurrence [Figure S8(b)]. Similar to the performance of SigFAM in the TCGA cohort, its Q1 has an application to separate out PCs that are least likely to relapse [Figure S8(c)]. Considering these results were obtained using an independent population which employed a different approach (microarray) to determine tumor transcriptomes, it serves to validate SigFAM as an effective signature in the prediction of PC recurrence.

SigFAM is a novel set of molecular biomarkers of PC recurrence

To further appreciate the biomarker potential of SigFAM, we performed a preliminary analysis of the 23 component genes, which predict PC recurrence in both the TCGA and MSKCC cohorts, for their relevance in PC and tumorigenesis in general (Table 3). Among these 23 genes, 16 have not been reported in PC and 6 genes (RELT, CLBA1, KIF9, CCDC137, VWA5B2, and SCML2) are unknown to function in tumorigenesis (Table 3). Among the rest 10 potential PC genes, UFM1 is downregulated in reference to FAM84B overexpression and is able to activate CDK5-associated tumor suppression[65]; both FAAP24 and TICRR function in DNA damage response, which is highly relevant in tumorigenesis[66,67]; while CRIP2 is upregulated in FAM84B xenografts, and may act to repress tumorigenesis[68]; RAB32, TRIM65, ADCY7, and ITGA11 promote tumorigenesis in gastric and endometrial adenocarcinoma,[69] bladder cancer,[70] acute myeloid leukemia,[71] and lung cancer[72]; LRWD1 plays a role in cell cycle progression[73]; and TIAM2 enhances Rac1 signaling[74] (Table 3).

There are seven other component genes that contribute to PC, including PPA2,[75] CHEK2,[76] FOXM1,[77] SYK,[78] ASF1B,[79] BGN,[80] and RAD54L[81] (Table 3). ASF1B enhances PC *via* activation of the PI3K/AKT pathway.[79] Upregulation of BGN is associated with PTEN deletion and poor prognosis in PC.[80] RAD54L is associated with CRPC development.[81] Collectively, the existing knowledge supports that SigFAM is a novel and robust signature of PC recurrence.

SigFAM independently predicts PC recurrence

To further investigate the stratification potential of SigFAM, we were able to show that SigFAM1 [hazard ratio (HR) 7.44, 95% confidence interval (CI) 4.76–11.62, $p < 2e^{-16}$] and SigFAM (HR 5.93, 95% CI 3.87–9.10, $p = 3e^{-16}$) are strong independent risk factors of PC recurrence after adjusting for age at diagnosis, Gleason scores, surgical margin, and T tumor stage (Table 4). Furthermore, 13 of the 27 SigFAM component genes, including 8 of 10 SigFAM1 component genes, remain independent risk factors in predicting PC recurrence after adjusting for age at diagnosis, GSs, surgical margin, and T tumor stage (Table 5). In view of their single gene status, their potentials to independently predict PC recurrence after adjusting for the aforementioned clinical factors further strengthened their potential in the evaluation of PC recurrence; these properties contribute to the robust nature of SigFAM in stratification of PCs at risk of recurrence.

Discussion

Although *FAM84B* resides in the most frequently amplified chromosome locus 8q24,[31,82] research on the protein's potential role in human cancers has been very limited, even considering the recent evidence for its association with esophageal squamous cell carcinoma[43,44] and PC.[45] We report here a thorough research effort supporting FAM84B's role in PC and the complex network through which FAM84B contributes to PC.

The properties of FAM84B in promoting PC progression are supported by its overexpression enhancing DU145 cell-derived oncogenic processes *in vitro* and *in vivo* (xenograft tumors and lung metastasis). Importantly, we described the first structural analysis that revealed a relationship of FAM84B with the HRASLS family. FAM84B shares a LRAT motif with the family (Figure 3), and conserved two histidine (His) residues among the catalytic triad (Figure 2). FAM84B is thus a remote HRASLS family member. All five members of the HRASLS family in humans have enzymatic activities of phospholipase $A_{1/2}$ and O-acyltrasferase[46]; HRASLS1-5 are able to suppress H-Ras-derived oncogenesis and are downregulated in human cancers[46]; evidence also supports a contribution of their enzymatic activities in tumor suppression.[46] Since the catalytic residue Cys is not conserved (Figure 2), FAM84B is unlikely to have either enzymatic activities, which implies that FAM84B facilitates

Table 3. The component genes of SigFAM[a].

Gene	Locus	Name	Role in PC/other tumorigenesis	Refs
UFM1[b]	13q13.3	Ubiquitin fold modifier 1	Unknown/could promoting tumor suppression	65
FAAP24[c]	19q13.11	Fanconi anemia core complex associated protein 24	Unknown/functioning in DNA damage response	66
PPA2[c]	4q24	Pyrophosphatase (inorganic) 2	Promoting PC	75
CHEK2[c]	22q12.1	Checkpoint kinase 2	Involved in PC	76
CRIP2[c]	14q32.33	Cysteine rich protein 2	Unknown/repression of tumorigenesis	68
RELT[c]	11q13.4	RELT, TNF receptor	Unknown/not clear	
RAB32[c]	6q24.3	RAB32, member Ras oncogene family	Unknown/promotion of esophageal carcinoma	69
CLBA1[c]	14q32.33	Clathrin binding box of aftiphilin containing 1	Unknown/unknown	
KIF9[c]	3q21.3	Kinesin family member 9	Unknown/not clear	
CCDC137[c]	17q25.3	Coiled-coil domain containing 137	Unknown/unknown	
TICRR[c]	15q26.1	TOPBP1 interacting checkpoint and replication regulator	Unknown/regulation of DNA replication *via* TOPBP1	67
VWA5B2[c]	3q27.1	Von Willebrand factor A domain containing 5B2	Unknown/unknown	
FOXM1[c]	12p13.33	Forkhead box M1	Well known to promote PC	77
LRWD1[c]	7q22.1	Leucine rich repeats and WD repeat domain containing 1	Unknown/promotion of cell cycle progression	73
SYK[c]	9q22.2	Spleen associated tyrosine kinase	Promotion of PC metastasis	78
SCML2[c]	Xp22.13	Scm polycomb group protein like 2	Unknown/not clear	
TRIM65[c]	17q25.1	Tripartite motif containing 65	Unknown/promoting bladder cancer	70
ADCY7[c]	16q12.1	Adenylate cyclase 7	Unknown/supporting acute myeloid leukemia	71
ASF1B[c]	19p13.12	Anti-silencing function 1B histone chaperone	Promotion of PC *via* the PI3K/AKT pathway/	79
BGN[c]	Xq28	Biglycan	Association with poor prognosis in PC	80
ITGA11[c]	15q23	Integrin subunit alpha 11	Unknown/promoting IGF2 signaling in lung cancer	72
RAD54L[c]	1p34.1	RAD54 like	Upregulated in CRPC	81
TIAM2[c]	6q25.2-3	T-Cell lymphoma invasion and metastasis 2	Unknown/stimulation of Rac1 signaling	74

[a]the component genes ($n = 23$) that predict PC recurrence in both the TCGA and MSKCC cohorts.
[b]downregulated genes.
[c]upregulated genes.
AKT, protein kinase B; CRPC, castration-resistant prostate cancer; IGF2, insulin like growth factor 2; PC, prostate cancer; PI3K, phosphoinositide 3-kinase; TNF, tumor necrosis factor; TOPBP1, DNA Topoisomerase II Binding Protein 1; WD, WD40 repeats or beta-transducin repeats.

Table 4. Univariate and multivariate Cox analysis of SigFAM and SigFAM1 for PC recurrence.

Factors	Univariate Cox analysis			Multivariate Cox analysis		
	HR	95% CI	*p* value	HR	95% CI	*p* value
Age[a]	1.03	0.995–1.06	0.0981	1.0[e] 0.996[f]	0.97–1.03 0.96–1.03	0.8680 0.8038
GS[b]	2.19	1.76–2.72	1.49e^{-12}***	1.63[e] 1.46[f]	1.25–2.12 1.11–1.92	0.0015** 0.0063**
Smargin[c]	2.25	1.48–3.41	0.000137***	0.99[e] 1.28[f]	0.61–1.60 0.81–2.01	0.9608 0.2909
TumStge[d]	3.68	2.08–6.51	8.19e^{-6}***	1.81[e] 1.54[f]	0.95–3.44 0.81–2.93	0.0710 0.1892
SigFAM1	7.44	4.76–11.62	$<$2e^{-16}***	4.17	2.49–6.98	5.32e^{-8}***
SigFAM	5.93	3.87–9.10	3e^{-16}***	3.66	2.03–5.57	2.44e^{-6}***

[a]age at diagnosis; [b]radical prostatectomy Gleason score; [c]surgical margin;
[d]tumor stages (0 for $\leqslant$T2; 1 for T3 and T4); [e]for SigFAM1; [f]for SigFAM.
CI, confidence interval; GS, Gleason score; HR, hazard ratio; PC, prostate cancer.

Ras signaling. This possibility is intriguing. Myc is well demonstrated to collaborate with Ras in tumorigenesis;[23–25] FAM84B is likely co-amplified with Myc owing to both genes bordering the 8q24.1 gene desert.[31,42,82–84] It is thus tempting to propose that the co-amplification facilitates Myc-Ras collaboration in part *via* FAM84B upregulation. Additionally, it is possible that FAM84B may reduce the actions of HRASLS1-5, thereby facilitating Ras signaling. As FAM84B may undergo intramolecular interaction *in vivo* (Figure 5), whether this is involved in FAM84B's action in PC remains to be explored. Further research is required to investigate the above concepts.

The above concepts seem to suggest indirect impacts of FAM84B on PC progression. This possibility is supported by the lack of effects in DU145 cell proliferation *in vitro* following FAM84B overexpression [Figure 1(b)] and the modest enhancement of tumor growth in the s.c. space and lung by ectopic FAM84B expression. Similar situation was also observed in BMI1; ectopic expression of BMI1 in MCF7 cells did not promote xenograft growth without other oncogenic manipulations.[48] BMI1 is a well demonstrated oncogene that collaborates with c-Myc and other oncogenes.[85–87] In this regard, to better understand FAM84B-facilitated oncogenesis, it is important to have knowledge on the potential mechanisms regulating FAM84B's actions.

While the mechanisms underlying FAM84B-facilitated prostate tumorigenesis are yet to be pinpointed, our research suggests that these mechanisms, although not limited to, regulate Golgi-to-ER processes, cell cycle checkpoints, mitochondria events, and protein metabolism (Figure 9). Among the Golgi-to-ER processes, the top pathways affected were those that regulate the Golgi-to-ER retrograde transport (Figure 10), which functions in tumorigenesis, including the epidermal growth factor receptor and Wnt signaling.[88,89] One of the interesting mitochondrial events affected is the respiratory electron transport and ATP synthesis (Figure 10), which is in line with the downregulation of the gene set of R-HAS-1428517 regulating the tricarboxylic acid cycle and respiratory electron transport (Figure 11). This suggests that FAM84B facilitates the Warburg metabolism or aerobic glycolysis in PC, the key pattern of cancer metabolism.[90]

While the mechanisms for FAM84B to alter these processes and their contributions to FAM84B-mediated prostate tumorigenesis are not clear, it is likely that the network affected by FAM84B is relevant to PC. This interpretation is supported by the derivation of the multigene signature SigFAM, and its sub-signature SigFAM1. Both signatures are novel and robustly stratify the high-risk population of PC recurrence in two independent cohorts. SigFAM can be explored for its

Table 5. Multivariate Cox analysis of the SigFAM component genes for DFS in PC.

Factors	HR	95% CI	*p* value
Age[a]	0.999–1.007[e]	(0.967–0.975)–(1.033–1.041)[f]	0.6609–0.9888[g]
GS[b]	1.717–1.930[e]	(1.324–.508)–(2.227–2.470)[f]	1.75e^{-7}–1.95e^{-5}***[g]
Smargin[c]	1.154–1.311[e]	(0.699–0.835)–(1.777–2.067)[f]	0.1452–0.6475[g]
TumStge[d]	1.748–2.017[e]	(0.924–1.069)–(3.306–3.805)[f]	0.0303*–0.0857[g]
UFM1	2.141	1.393–3.292	0.000521***
FAAP24	1.772	1.095–2.868	0.01999*
CHEK2	1.654	1.069–2.532	0.0236*
RELT	1.671	1.055–2.648	0.0287*
CLBA1	2.093	1.350–3.245	0.000969***
KIF9	1.684	1.112–2.549	0.0138*
CCDC137	1.647	1.059–2.561	0.0267*
VWA5B2	1.869	1.219–2.867	0.00416**
FOXM1	1.630	1.036–2.563	0.0347*
LRWD1	1.880	1.232–2.870	0.00341**
TRIM65	2.384	1.560–3.643	5.95e^{-5}***
ASF1	1.798	1.139–2.840	0.0119*
RAD54L	1.791	1.139–2.816	0.0117*

[a]age at diagnosis; [b]radical prostatectomy Gleason score; [c]surgical margin; [d]tumor stages (0 for ⩽T2; 1 for T3 and T4); [e]the range of HR in multivariate analyses with the individual components genes; [f]the range of 95% CI in multivariate analyses with the individual components genes; [g]the largest *p* values in multivariate analyses with the individual components genes; *$p < 0.05$; **$p < 0.01$; ***$p < 0.001$; the TCGA dataset was used in the analyzes.
CI, confidence interval; GS, Gleason score; HR, hazard ratio; PC, prostate cancer; TCGA, The Cancer Genome Atlas.

clinical application to improve patient management. Furthermore, the novel component genes identified may open new branches in PC research. Finally, it is likely that the results obtained in this research are not limited to PC. It will be interesting to investigate the involvement of FAM84B in cancers produced from those tissues expressing the FAM84B protein at the medium to high levels, like endometrium, cervix, breast, kidney, liver, lung, and others (Figure S5).

We have examined FAM84B-derived oncogenic effects with multiple systems including functional studies (*in vitro* and *in vivo*), mechanistic approaches (RNA sequencing with duplicates), and clinical significance investigations (modeling FAM84B-associated DEGs). However, this study has several limitations. (1) Horizontally expanding the knowledge obtained from this study in other PC cell lines, particularly androgen-dependent PC cells like LNCaP cells will strengthen this study, if similar effects are demonstrated. However, we like to emphasize that negative results will not weaken this investigation. (2) The association between the identified network or DEGs and FAM84B functions warrant further investigation; this research likely requires a major effort. (3) The multigene signature built here certainly requires further tests; how this signature is related with FAM84B functions should be investigated in future studies.

Acknowledgements

The results shown here are in part based upon data generated by the TCGA Research Network (http://cancergenome.nih.gov/).

Funding

This work was supported in part by a grant from Cancer Research Society to D.T. and funds from Urological Cancer Center for Research and Innovation (UCCRI). Y.G. is supported by studentship provided by Ontario Graduate Student Fellowship and Research Institute of St Joe's Hamilton.

Conflict of interest statement

The authors declare that there is no conflict of interest.

Supplemental material

Supplemental material for this article is available online.

References

1. Ferlay J, Soerjomataram I, Dikshit R, *et al.* Cancer incidence and mortality worldwide: sources, methods and major patterns in GLOBOCAN 2012. *Int J Cancer* 2015; 136: E359–E386.
2. Heidenreich A, Bastian PJ, Bellmunt J, *et al.* EAU guidelines on prostate cancer. Part II: treatment of advanced, relapsing, and castration-resistant prostate cancer. *Eur Urol* 2014; 65: 467–479.
3. Egevad L, Delahunt B, Srigley JR, *et al.* International Society of Urological Pathology (ISUP) grading of prostate cancer - An ISUP consensus on contemporary grading. *APMIS* 2016; 124: 433–435.
4. Gordetsky J and Epstein J. Grading of prostatic adenocarcinoma: current state and prognostic implications. *Diagn Pathol* 2016; 11: 25.
5. Epstein JI, Zelefsky MJ, Sjoberg DD, *et al.* A contemporary prostate cancer grading system: a validated alternative to the gleason score. *Eur Urol* 2016; 69: 428–435.
6. Zaorsky NG, Raj GV, Trabulsi EJ, *et al.* The dilemma of a rising prostate-specific antigen level after local therapy: what are our options? *Semin Oncol* 2013; 40: 322–336.
7. Shipley WU, Seiferheld W, Lukka HR, *et al.* Radiation with or without antiandrogen therapy in recurrent prostate cancer. *N Engl J Med* 2017; 376: 417–428.
8. Rosenberg J and Small EJ. Prostate cancer update. *Curr Opin Oncol* 2003; 15: 217–221.
9. Ross JS. The androgen receptor in prostate cancer: therapy target in search of an integrated diagnostic test. *Adv Anat Pathol* 2007; 14: 353–357.
10. Semenas J, Allegrucci C, Boorjian SA, *et al.* Overcoming drug resistance and treating advanced prostate cancer. *Curr Drug Targets* 2012; 13: 1308–1323.
11. Ojo D, Lin X, Wong N, *et al.* Prostate cancer stem-like cells contribute to the development of castration-resistant prostate cancer. *Cancers (Basel)* 2015; 7: 2290–2308.
12. de Bono JS, Logothetis CJ, Molina A, *et al.* Abiraterone and increased survival in metastatic prostate cancer. *N Engl J Med* 2011; 364: 1995–2005.
13. Scher HI, Fizazi K, Saad F, *et al.* Increased survival with enzalutamide in prostate cancer after chemotherapy. *N Engl J Med* 2012; 367: 1187–1197.
14. Chaturvedi S and Garcia JA. Novel agents in the management of castration resistant prostate cancer. *J Carcinog* 2014; 13: 5.
15. Drake CG. Prostate cancer as a model for tumour immunotherapy. *Nat Rev Immunol* 2010; 10: 580–593.
16. Mei W, Gu Y, Jiang Y, *et al.* Circulating cell-free DNA is a potential prognostic biomarker of metastatic castration-resistant prostate cancer for taxane therapy. *AME Med J* 2018; 3: 1–5.
17. Abate-Shen C and Shen MM. Molecular genetics of prostate cancer. *Gen Dev* 2000; 14: 2410–2434.
18. Schrecengost R and Knudsen KE. Molecular pathogenesis and progression of prostate cancer. *Semin Oncol* 2013; 40: 244–258.
19. Nag A and Smith RG. Amplification, rearrangement, and elevated expression of c-myc in the human prostatic carcinoma cell line LNCaP. *Prostate* 1989; 15: 115–122.
20. Jenkins RB, Qian J, Lieber MM, *et al.* Detection of c-myc oncogene amplification and chromosomal anomalies in metastatic prostatic carcinoma by fluorescence in situ hybridization. *Cancer Res* 1997; 57: 524–531.
21. Hawksworth D, Ravindranath L, Chen Y, *et al.* Overexpression of C-MYC oncogene in prostate cancer predicts biochemical recurrence. *Prostate Cancer Prostatic Dis* 2010; 13: 311–315.
22. Sato K, Qian J, Slezak JM, *et al.* Clinical significance of alterations of chromosome 8 in high-grade, advanced, nonmetastatic prostate carcinoma. *J Natl Cancer Inst* 1999; 91: 1574–1580.
23. Land H, Parada LF and Weinberg RA. Tumorigenic conversion of primary embryo

fibroblasts requires at least two cooperating oncogenes. *Nature* 1983; 304: 596–602.

24. Leone G, DeGregori J, Sears R, *et al*. Myc and Ras collaborate in inducing accumulation of active cyclin E/Cdk2 and E2F. *Nature* 1997; 387: 422–426.
25. Wang C, Lisanti MP and Liao DJ. Reviewing once more the c-myc and Ras collaboration: converging at the cyclin D1-CDK4 complex and challenging basic concepts of cancer biology. *Cell Cycle* 2011; 10: 57–67.
26. Thompson TC, Southgate J, Kitchener G, *et al*. Multistage carcinogenesis induced by ras and myc oncogenes in a reconstituted organ. *Cell* 1989; 56: 917–930.
27. Amundadottir LT, Sulem P, Gudmundsson J, *et al*. A common variant associated with prostate cancer in European and African populations. *Nat Genet* 2006; 38: 652–658.
28. Easton DF, Pooley KA, Dunning AM, *et al*. Genome-wide association study identifies novel breast cancer susceptibility loci. *Nature* 2007; 447: 1087–1093.
29. Freedman ML, Haiman CA, Patterson N, *et al*. Admixture mapping identifies 8q24 as a prostate cancer risk locus in African-American men. *Proc Natl Acad Sci USA* 2006; 103: 14068–14073.
30. Haiman CA, Le Marchand L, Yamamato J, *et al*. A common genetic risk factor for colorectal and prostate cancer. *Nat Genet* 2007; 39: 954–956.
31. Haiman CA, Patterson N, Freedman ML, *et al*. Multiple regions within 8q24 independently affect risk for prostate cancer. *Nat Genet* 2007; 39: 638–644.
32. Braem MG, Schouten LJ, Peeters PH, *et al*. Genetic susceptibility to sporadic ovarian cancer: a systematic review. *BBA* 2011; 1816: 132–146.
33. Haerian MS, Baum L and Haerian BS. Association of 8q24.21 loci with the risk of colorectal cancer: a systematic review and meta-analysis. *J Gastroenterol Hepatol* 2011; 26: 1475–1484.
34. Broderick P, Carvajal-Carmona L, Pittman AM, *et al*. A genome-wide association study shows that common alleles of SMAD7 influence colorectal cancer risk. *Nat Genet* 2007; 39: 1315–1317.
35. Tomlinson I, Webb E, Carvajal-Carmona L, *et al*. A genome-wide association scan of tag SNPs identifies a susceptibility variant for colorectal cancer at 8q24.21. *Nat Genet* 2007; 39: 984–988.
36. Hindorff LA, Gillanders EM and Manolio TA. Genetic architecture of cancer and other complex diseases: lessons learned and future directions. *Carcinogenesis* 2011; 32: 945–954.
37. Vargas AC, Lakhani SR and Simpson PT. Pleomorphic lobular carcinoma of the breast: molecular pathology and clinical impact. *Future Oncol* 2009; 5: 233–243.
38. Garcia-Closas M and Chanock S. Genetic susceptibility loci for breast cancer by estrogen receptor status. *Clin Cancer Res* 2008; 14: 8000–8009.
39. Schumacher FR, Feigelson HS, Cox DG, *et al*. A common 8q24 variant in prostate and breast cancer from a large nested case-control study. *Cancer Res* 2007; 67: 2951–2956.
40. Nakagawa H, Akamatsu S, Takata R, *et al*. Prostate cancer genomics, biology, and risk assessment through genome-wide association studies. *Cancer Sci* 2012; 103: 607–613.
41. Gudmundsson J, Sulem P, Manolescu A, *et al*. Genome-wide association study identifies a second prostate cancer susceptibility variant at 8q24. *Nat Genet* 2007; 39: 631–637.
42. Yeager M, Orr N, Hayes RB, *et al*. Genome-wide association study of prostate cancer identifies a second risk locus at 8q24. *Nat Genet* 2007; 39: 645–649.
43. Cheng C, Cui H, Zhang L, *et al*. Genomic analyses reveal FAM84B and the NOTCH pathway are associated with the progression of esophageal squamous cell carcinoma. *GigaScience* 2016; 5: 1.
44. Hsu FM, Cheng JC, Chang YL, *et al*. Circulating mRNA profiling in esophageal squamous cell carcinoma identifies FAM84B as a biomarker in predicting pathological response to neoadjuvant chemoradiation. *Sci Rep* 2015; 5: 10291.
45. Wong N, Gu Y, Kapoor A, *et al*. Upregulation of FAM84B during prostate cancer progression. *Oncotarget* 2017; 8: 19218–19235.
46. Mardian EB, Bradley RM and Duncan RE. The HRASLS (PLA/AT) subfamily of enzymes. *J Biomed Sci* 2015; 22: 99.
47. He L, Fan C, Kapoor A, *et al*. Alpha-Mannosidase 2C1 attenuates PTEN function in prostate cancer cells. *Nat Commun* 2011; 2: 307.
48. Ojo D, Lin X, Wu Y, *et al*. Polycomb complex protein BMI1 confers resistance to tamoxifen in estrogen receptor positive breast cancer. *Cancer Lett* 2018; 426: 4–13.
49. He L, Ingram A, Rybak AP, *et al*. Shank-interacting protein-like 1 promotes tumorigenesis via PTEN inhibition in human tumor cells. *J Clin Investig* 2010; 120: 2094–2108.

50. Yan J, Ojo D, Kapoor A, *et al.* Neural cell adhesion protein CNTN1 promotes the metastatic progression of prostate cancer. *Cancer Res* 2016; 76: 1603–1614.

51. Wei F, Hao P, Zhang X, *et al.* Etoposide-induced DNA damage affects multiple cellular pathways in addition to DNA damage response. *Oncotarget* 2018; 9: 24122–24139.

52. Yu G and He QY. ReactomePA: an R/Bioconductor package for reactome pathway analysis and visualization. *Mol Biosyst* 2016; 12: 477–479.

53. Cerami E, Gao J, Dogrusoz U, *et al.* The cBio cancer genomics portal: an open platform for exploring multidimensional cancer genomics data. *Cancer Discov* 2012; 2: 401–404.

54. Gao J, Aksoy BA, Dogrusoz U, *et al.* Integrative analysis of complex cancer genomics and clinical profiles using the cBioPortal. *Sci Signal* 2013; 6: pl1.

55. Ren X, Lin J, Jin C, *et al.* Solution structure of the N-terminal catalytic domain of human H-REV107—a novel circular permutated NlpC/P60 domain. *FEBS Lett* 2010; 584: 4222–4226.

56. Cohen-Solal KA, Boregowda RK and Lasfar A. RUNX2 and the PI3K/AKT axis reciprocal activation as a driving force for tumor progression. *Mol Cancer* 2015; 14: 137.

57. Song G, Ouyang G and Bao S. The activation of Akt/PKB signaling pathway and cell survival. *J Cell Mol Med* 2005; 9: 59–71.

58. Madakashira BP and Sadler KC. DNA methylation, nuclear organization, and cancer. *Front Genet* 2017; 8: 76.

59. Jiang Y, Mei W, Gu Y, *et al.* Construction of a set of novel and robust gene expression signatures predicting prostate cancer recurrence. *Mol Oncol* 2018; 12: 1559–1578.

60. Lin X, Gu Y, Kapoor A, *et al.* Overexpression of MUC1 and genomic alterations in its network associate with prostate cancer progression. *Neoplasia* 2017; 19: 857–867.

61. Ojo D, Seliman M and Tang D. Signatures derived from increase in SHARPIN gene copy number are associated with poor prognosis in patients with breast cancer. *BBA Clin* 2017; 8: 56–65.

62. Cuzick J, Swanson GP, Fisher G, *et al.* Prognostic value of an RNA expression signature derived from cell cycle proliferation genes in patients with prostate cancer: a retrospective study. *Lancet Oncol* 2011; 12: 245–255.

63. Cooperberg MR, Simko JP, Cowan JE, *et al.* Validation of a cell-cycle progression gene panel to improve risk stratification in a contemporary prostatectomy cohort. *J Clin Oncol* 2013; 31: 1428–1434.

64. Taylor BS, Schultz N, Hieronymus H, *et al.* Integrative genomic profiling of human prostate cancer. *Cancer Cell* 2010; 18: 11–22.

65. Daniel J and Liebau E. The ufm1 cascade. *Cells* 2014; 3: 627–638.

66. Huang M, Kim JM, Shiotani B, *et al.* The FANCM/FAAP24 complex is required for the DNA interstrand crosslink-induced checkpoint response. *Mol Cell* 2010; 39: 259–268.

67. Sansam CG, Goins D, Siefert JC, *et al.* Cyclin-dependent kinase regulates the length of S phase through TICRR/TRESLIN phosphorylation. *Genes Dev* 2015; 29: 555–566.

68. Cheung AK, Ko JM, Lung HL, *et al.* Cysteine-rich intestinal protein 2 (CRIP2) acts as a repressor of NF-kappaB-mediated proangiogenic cytokine transcription to suppress tumorigenesis and angiogenesis. *Proc Natl Acad Sci USA* 2011; 108: 8390–8395.

69. Shibata D, Mori Y, Cai K, *et al.* RAB32 hypermethylation and microsatellite instability in gastric and endometrial adenocarcinomas. *Int J Cancer* 2006; 119: 801–806.

70. Wei WS, Chen X, Guo LY, *et al.* TRIM65 supports bladder urothelial carcinoma cell aggressiveness by promoting ANXA2 ubiquitination and degradation. *Cancer Lett* 2018; 435: 10–22.

71. Li C, Xie J, Lu Z, *et al.* ADCY7 supports development of acute myeloid leukemia. *Biochem Biophys Res Commun* 2015; 465: 47–52.

72. Zhu CQ, Popova SN, Brown ER, *et al.* Integrin alpha 11 regulates IGF2 expression in fibroblasts to enhance tumorigenicity of human non-small-cell lung cancer cells. *Proc Natl Acad Sci USA* 2007; 104: 11754–11759.

73. Wang CY, Hong YH, Syu JS, *et al.* LRWD1 Regulates microtubule nucleation and proper cell cycle progression in the human testicular embryonic carcinoma cells. *J Cell Biochem* 2018; 119: 314–326.

74. Yen WH, Ke WS, Hung JJ, *et al.* Sp1-mediated ectopic expression of T-cell lymphoma invasion and metastasis 2 in hepatocellular carcinoma. *Cancer Med* 2016; 5: 465–477.

75. Pang J, Liu WP, Liu XP, *et al.* Profiling protein markers associated with lymph node metastasis

in prostate cancer by DIGE-based proteomics analysis. *J Proteome Res* 2010; 9: 216–226.

76. Jividen K, Kedzierska KZ, Yang CS, *et al.* Genomic analysis of DNA repair genes and androgen signaling in prostate cancer. *BMC Cancer* 2018; 18: 960.
77. Aytes A, Mitrofanova A, Lefebvre C, *et al.* Cross-species regulatory network analysis identifies a synergistic interaction between FOXM1 and CENPF that drives prostate cancer malignancy. *Cancer Cell* 2014; 25: 638–651.
78. Ghotra VP, He S, van der Horst G, *et al.* SYK is a candidate kinase target for the treatment of advanced prostate cancer. *Cancer Res* 2015; 75: 230–240.
79. Han G, Zhang X, Liu P, *et al.* Knockdown of anti-silencing function 1B histone chaperone induces cell apoptosis via repressing PI3K/Akt pathway in prostate cancer. *Int J Oncol* 2018; 53: 2056–2066.
80. Jacobsen F, Kraft J, Schroeder C, *et al.* Up-regulation of biglycan is associated with poor prognosis and PTEN deletion in patients with prostate cancer. *Neoplasia* 2017; 19: 707–715.
81. Li L, Karanika S, Yang G, *et al.* Androgen receptor inhibitor-induced "BRCAness" and PARP inhibition are synthetically lethal for castration-resistant prostate cancer. *Sci Signal* 2017; 10.
82. Ghoussaini M, Song H, Koessler T, *et al.* Multiple loci with different cancer specificities within the 8q24 gene desert. *J Natl Cancer Inst* 2008; 100: 962–966.
83. Al Olama AA, Kote-Jarai Z, Giles GG, *et al.* Multiple loci on 8q24 associated with prostate cancer susceptibility. *Nat Genet* 2009; 41: 1058–1060.
84. Gudmundsson J, Sulem P, Gudbjartsson DF, *et al.* A study based on whole-genome sequencing yields a rare variant at 8q24 associated with prostate cancer. *Nat Genet* 2012; 44: 1326–1329.
85. Haupt Y, Alexander WS, Barri G, *et al.* Novel zinc finger gene implicated as myc collaborator by retrovirally accelerated lymphomagenesis in E mu-myc transgenic mice. *Cell* 1991; 65: 753–763.
86. van Lohuizen M, Verbeek S, Scheijen B, *et al.* Identification of cooperating oncogenes in E mu-myc transgenic mice by provirus tagging. *Cell* 1991; 65: 737–752.
87. Lin X, Ojo D, Wei F, *et al.* A novel aspect of tumorigenesis-BMI1 functions in regulating DNA damage response. *Biomolecules* 2015; 5: 3396–3415.
88. Wang YN, Wang H, Yamaguchi H, *et al.* COPI-mediated retrograde trafficking from the Golgi to the ER regulates EGFR nuclear transport. *Biochem Biophys Res Commun* 2010; 399: 498–504.
89. Yu J, Chia J, Canning CA, *et al.* WLS retrograde transport to the endoplasmic reticulum during Wnt secretion. *Dev Cell* 2014; 29: 277–291.
90. Wong N, Ojo D, Yan J, *et al.* PKM2 contributes to cancer metabolism. *Cancer Lett* 2015; 356: 184–191.